Hindawi
Molecular Imaging
Volume 2023, Article ID 4131117, 22 pages
https://doi.org/10.1155/2023/4131117

Review Article

Magnetic Particle Imaging in Vascular Imaging, Immunotherapy, Cell Tracking, and Noninvasive Diagnosis

Prashant Chandrasekharan,[1] **Renesmee Kuo**,[1] **K. L. Barry Fung**,[1] **Chinmoy Saayujya**,[2] **Jacob Bryan**,[1] **Mariam Yousuf**,[1] **Benjamin Fellows**,[1] **Caylin Colson**,[1] **Quincy Huynh**,[2] **Owen Doyle**,[1] **Allison Hartley**,[1] **Khadija Yousuf**,[1] **Patrick Goodwill**,[3] **and Steven Conolly**[1,2]

[1]*Department of Bioengineering, Berkeley, University of California Berkeley, CA 94720, USA*
[2]*Department of Electrical Engineering and Computer Sciences, University of California, Berkeley, CA 94720, USA*
[3]*Magnetic Insight, Alameda, CA, USA*

Correspondence should be addressed to Prashant Chandrasekharan; prashantc@berkeley.edu

Received 18 December 2022; Revised 20 February 2023; Accepted 28 February 2023; Published 15 March 2023

Academic Editor: Alexei Bogdanov

Copyright © 2023 Prashant Chandrasekharan et al. This is an open access article distributed under the Creative Commons Attribution License, which permits unrestricted use, distribution, and reproduction in any medium, provided the original work is properly cited.

Magnetic particle imaging (MPI) is a new tracer-based imaging modality that is useful in diagnosing various pathophysiology related to the vascular system and for sensitive tracking of cytotherapies. MPI uses nonradioactive and easily assimilated nanometer-sized iron oxide particles as tracers. MPI images the nonlinear Langevin behavior of the iron oxide particles and has allowed for the sensitive detection of iron oxide-labeled therapeutic cells in the body. This review will provide an overview of MPI technology, the tracer, and its use in vascular imaging and cytotherapies using molecular targets.

1. Introduction

Magnetic particle imaging (MPI) is a relatively new imaging modality that images the spatial distribution of superparamagnetic iron oxide nanoparticles as a tracer [1–4]. MPI was first developed by Gleich & Weizenecker from the Philips research center in Hamburg [5] and has ever since seen rapid growth in various forms, including hardware [6–9], image acquisition and reconstruction [10–15], tracer developments [16–22], and implementation in preclinical translational research [23–27].

Magnetic particle imaging is not to be confused with magnetic resonance imaging (MRI) [4]. Though some of the iron oxide tracers used for MRI can also be used for MPI, the working principles of MPI and MRI are entirely different. In MPI, the superparamagnetic iron oxide (SPIO) tracers are directly imaged, whereas in MRI, the paramagnetic proton that comes under the influence of the magnetized SPIO tracer is measured. This influence results in a change in the T2∗ times of proton relaxation resulting in a negative contrast in MRI. However, MPI generates a positive signal from the instantaneous location of the SPIO tracer. In Figure 1, we highlight some preclinical MPI images of immense diagnostic and translational value. These images consist solely of tracer particles, making them similar to images produced in nuclear medicine. MPI is particularly useful for vascular imaging [28–31] and for tracking cytotherapies, such as red blood cells (RBCs) [32], stem cells [33–35], and white blood cells (WBCs) [23, 36, 37], all without any radiation.

Tracers for MPI consist of nanosized superparamagnetic iron oxide nanoparticles administered intravenously (i.v.). MPI tracers coated with polyethylene glycol resist opsonization and compartmentalize in the blood plasma. This results in a longer circulation time, which enables highly sensitive angiograms that could detect gastrointestinal bleeding as shown in Figure 1(b). Furthermore, MPI tracers with antibodies can selectively bind to molecular targets in circulating

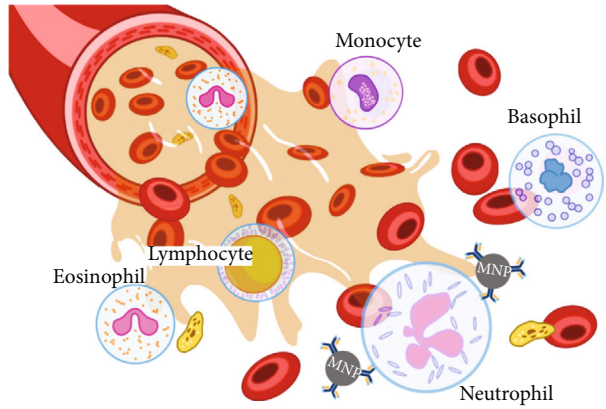

(a) MPI tracks immune cells homing to infection, inflammation, and cancer

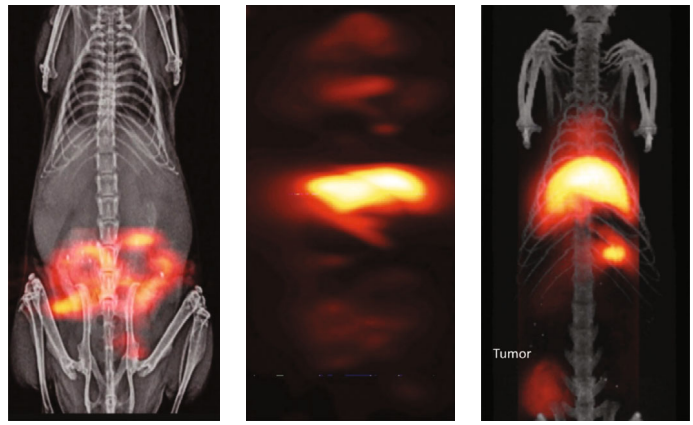

(b) Vascular imaging (c) Molecular imaging (d) Cancer imaging

Figure 1: MPI overview: magnetic particle imaging is a new, noninvasive, and nonradioactive tracer-based imaging technology for imaging pathologies associated with vascular defects, cell tracking, and molecular imaging. (a) Intravenously administered tracers of MPI can be engineered to either partition in the blood plasma or tag to a specific subset of immune cells using molecular targets (MNP: magnetic nanoparticles). (b) Long-circulating tracers in MPI can be used to acquire highly sensitive angiograms that could detect gastrointestinal bleeding shown here. MPI images of bleed hot spots can be observed in the abdomen overlaid over a projection X-ray for anatomical reference. (Adapted with permission from Yu et al., ACS Nano, 2017. Copyright (2017) American Chemical Society) [27] (c) Furthermore, MPI tracers with antibodies can selectively bind to molecular targets in circulating immune cells, such as neutrophils, and allow for sensitive tracking of therapeutic cells. (Reproduced under the Creative Common license) (d) MPI can image malformed angiogenic blood vessels in tumors due to enhanced permeation and retention (image overlaid over CT data for anatomical reference) (adapted with permission from Yu et al., Nano Letters, 2017. Copyright (2017) American Chemical Society [38]).

immune cells, such as neutrophils, and allow for sensitive tracking of therapeutic cells (Figure 1(c)). MPI can image malformed angiogenic blood vessels in tumors due to enhanced permeation and retention (Figure 1(d)).

In this review article, we will introduce the chemistry and working principle behind the tracers of MPI, followed by a brief introduction to image acquisition using the tracers. We will finally highlight some examples of vascular and cellular imaging of theranostic value using MPI.

2. Tracers for MPI

MPI is a tracer-based imaging modality, and the magnetic properties of tracers greatly influence the sensitivity and resolution of the images. Superparamagnetic iron oxide nanoparticles or SPIOs have long been used in biomedicine, as contrast agents in MRI, as an iron supplement for treating anemic patients, and for hyperthermia-based treatment involving inductive heating. Unlike small molecule tracers used in nuclear medicine, tracers for MPI are similar to ^{99m}Tc-sulfur colloids, except MPI tracers are nonradioactive (Figure 2).

SPIOs are superparamagnetic and exhibit the Langevin physics which is crucial for MPI (Figure 3(a)). Ferromagnetic materials of iron oxide that are confined to the "nanometer" dimension between approximately 3 and 30 nm near the spherical diameter behave superparamagnetic. Superparamagnetic materials are strongly magnetized in the presence of an externally applied magnetic field and can switch the direction of magnetization with the switch in the direction

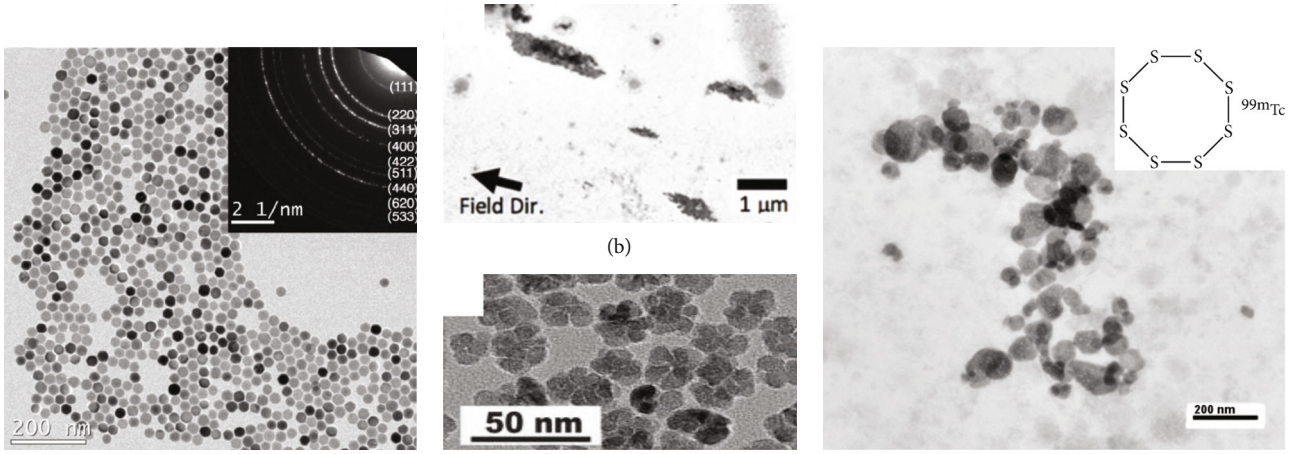

(a) (b) (c) (d)

Figure 2: Unlike the small molecule metal chelators used in nuclear medicine which are typical 1-2 nm in size, MPI uses colloids of (a–c) iron oxide nanoparticles (SPIO) with core sizes of 4–28 nm [27]. For this reason, many MPI applications studied thus far bears a close resemblance to nuclear medicine studies using (adapted with permission from Yu et al., ACS Nano, 2017. Copyright (2017) American Chemical Society, Chandrasekharan et al., Theranostics, 2020 [39]; Tay et al., Small Methods, 2021 [40]) (d) ^{99m}Tc-Sulfur colloids [41], but with no radiation nor any radioactive decay. Signals from the MPI tracer persist until the SPIO particles are enzymatically hydrolyzed and cleared (Reproduced with permission from Michenfelder MM et al., J Nucl Med Technol, 2014).

of the applied field. SPIOs have zero remanences and coercivity, which are needed for spatial localization using MPI. The derivative of Langevin is the point-spread function of the image in MPI, with the full width at half maximum (FWHM) corresponding to the magnetic resolution (Figure 3(b)). The saturation magnetization and the slope of the linear portion of Langevin are critical in determining the sensitivity and resolution of particles for MPI [1–3, 18, 22].

The magnetic property of the tracer depends on the size and crystalline nature of the iron oxide particles, which is influenced by the route of synthesis. Many of the commercial SPIO particles are prepared by a bottom-up approach. In the bottom-up approach of SPIO preparation, Fe^{2+} and Fe^{3+} salts are mixed under strongly basic or acidic conditions. The salts precipitate to form a colloidal crystal of iron oxide. This reaction referred to as the Schikorr reaction, has been the classical method for preparing a variety of commercially available SPIOs [44, 45]. The resulting products of the Schikorr reaction usually contain mixed phases of oxides of iron such as FeO (Wüstite), Fe_2O_3 (hematite), and Fe_3O_4 (Magnetite). In common practice, the iron oxides formed are oxidized further to improve the magnetic property of the product [17, 46, 47].

In Table 1, we have listed the details of some commercially available SPIO tracers, including their crystalline phase and MPI properties. Feraheme [48] and Resovist [49] are two of the tracers prepared by the Schikorr reaction detailed above [44], and both have an average particle core size of approximately 5 nm. Feraheme particles have maghemite (γ-Fe_2O_3) as a crystalline phase, while X-ray diffraction studies in Resovist show a mixed magnetite (Fe_3O_4) and maghemite (γ-Fe_2O_3) crystalline phase. The susceptibility (χ) of the crystalline phase of magnetite is almost 1.5–2 times higher than that of maghemite, with magnetite particles showing better MPI signal and resolution [50]. LodeSpin nanoparticles from the University of Washington were prepared by a thermal decomposition process of the organometallic precursor in a controlled chemical environment. The thermal decomposition process allows for greater control of the size and oxidative state of iron oxide crystals. LodeSpin particles with long blood circulation time have a sensitivity value of 3 ng and a 0.83 mm resolution in a 7 T/m/μ_0 gradient field-free line MPI scanner (Table 1) [27, 38]. LodeSpin particles have pure-phase magnetite (inset Figure 2(a) represents a selected area electron diffraction pattern showing crystal morphology and characteristic spinel diffraction rings) core having the highest magnetic susceptibility [16]. Apart from the crystalline phase, the size of the iron oxide nanoparticles influences the resolution and sensitivity. The Langevin equations of physics predict a cubic improvement (resolution, FWHM scales ~1/(particle diameter)^3). But in reality, the measured resolution is affected due to particle relaxation, which is merely a time delay τ for the particle magnetization to align with the externally applied field [51]. Factors like excitation frequency and amplitude can further affect the resolution and sensitivity of MPI [52].

Attempts have been made to synthesize magnetic nanoparticles with better resolution and sensitivity. Zero-valent iron oxide nanoparticles are considered to have the highest magnetic susceptibility compared to various iron-crystal forms. However, the iron-zero state is not very stable and would quickly oxidize at room temperature and atmospheric pressure. Researchers from Monash University developed zero-valent iron oxide nanoparticles with an approximately 5-8 nm core and vectorized it with an approximately 3 nm thick iron oxide shell [21]. The iron oxide shell provided a

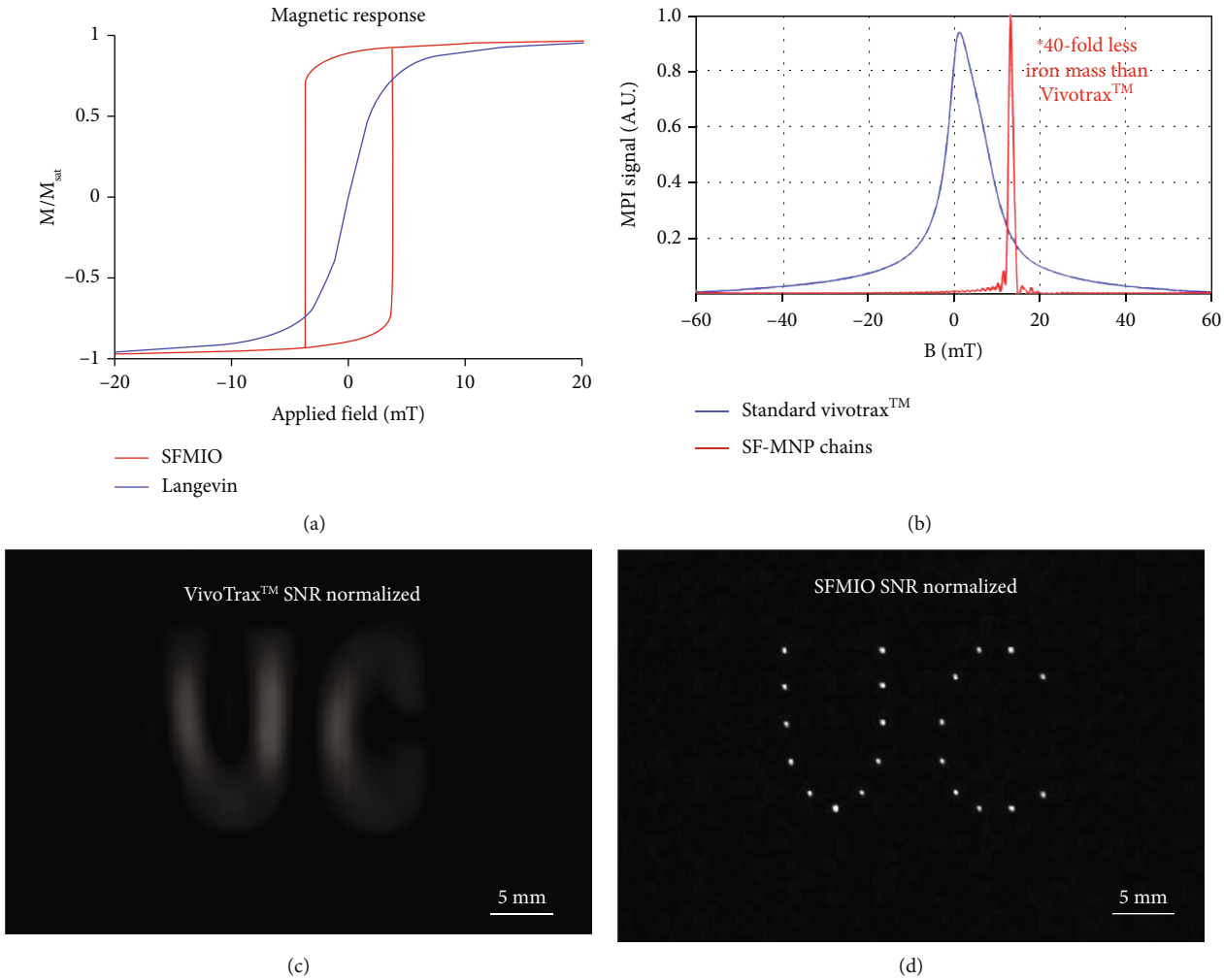

Figure 3: Tracers of MPI obey (a) Langevin physics (blue line). At UC Berkeley, we have discovered that SPIO particles interact to create a new form of magnetic behavior which provides a step-like change in response to a magnetic field (red line). We coined this new type of particle as superferromagnetic iron oxide nanoparticles (SFMIO). (b) The step response-like behavior of SFMIO particles to the applied field provides high resolution and higher signal compared to VivoTrax™ as shown by the point-spread function (PSF) of the particles. (Reproduced with permission from Tay et al., Small Methods, 2021 [40]) (c) MPI images of VivoTrax™ filled in capillary tubes to create a pointillism phantom acquired using a 6.3 T/m field-free line MPI scanner versus (d) SFMIO particles. SFMIOs have been shown to improve the resolution of MPI to 100 microns, a 10-fold improvement compared to commercial nanoparticles [40, 42, 43].

Table 1: Commercially available SPIO tracers used for MPI had their resolution and sensitivity measured using an arbitrary wave relaxometer [1, 40] (reproduced with permission from Chandrasekharan et al. [1]).

Commercial particles	Crystal phase/size	MPI resolution/sensitivity
Feraheme	γ-Fe_2O_3 Maghemite/6-7 nm	5.6 mm/77 ng
Resovist (Ferucarbotran)	Magnetite (Fe_3O_4) & Maghemite (Fe_2O_3)/3-5 nm	1.4 mm/12 ng
LodeSpin lab	Magnetite (Fe_3O_4)/29 nm	0.83 mm/3 ng
Superferromagnetic particles	Interacting	~0.1 mm/10-fold better sensitivity [40]

protective layer over the zero-valent iron. The particles had an MPI signal and resolution comparable to ferucarbotran. Other approaches have been carried out to improve the crystalline anisotropy of the nanoparticle either using doped iron oxide or cube-shaped iron oxide nanoparticles [53, 54]. The improved anisotropy provides a great advantage for MPI-guided hysteresis heating of the nanoparticles, commonly referred to as magnetic fluid hyperthermia [19, 25, 55–57].

Recently, UC Berkeley collaborated with the University of Florida to develop a new class of high-resolution MPI tracers called superferromagnetism (SFMIO). SFMIO nanoparticles transiently interact to form chains that flip instantaneously and provide a sharp transition of the magnetic

field vector with the change in applied field (dM(t)/dH(t)) [40]. This sharp transition provides a 10-fold boost in MPI resolution compared to commercial MPI tracers at a 7 T/m magnetic field gradient (Figure 3(d)). The high-resolution SFMIO nanoparticles will allow for the scale-up of preclinical MPI scanners to human-size scanners by reducing the gradient strength needed by 10-fold. A mere 1 T/m gradient MPI could provide 1-mm resolution images using SFMIO particles, which is the nominal resolution of a clinical SPECT or PET scanner. Since gradient hardware cost scales quadratically with field strength, SFMIO nanoparticles could reduce the gradient cost, remove any hardware constraints, and make human MPI scanners affordable.

SPIOs are colloidally stabilized using biocompatible materials, such as carboxydextran (polyglucose in the case of Feraheme and Resovist) or polyethylene glycol (PEG) (in the case of LodeSpin) and reconstituted in a pharmaceutical adjuvant for intravenous administration. For diagnostic purposes, SPIOs can be repurposed within biomolecules, such as chylomicrons [26], red blood cells [32, 58], white blood cells [23, 36, 59], stem cells [33–35], exosomes [60], and synaptic vesicles [61], and can be used for functional and metabolic imaging (see Figure 4). SPIO tracers developed so far have been approved only as a supplement for anemia and an off-label MRI contrast agent. Tracers for MPI could benefit from having a custom iron oxide core built over a previously FDA-approved biocompatible formulation. Such tracers can be fast-tracked for first-in-human clinical use through device exemption, owing to the overall diagnostic benefit of magnetic particle imaging (MPI). In the following sections, we will discuss some key benefits of MPI that have been proven in preclinical setups for modern-day nanotheranostics.

3. Magnetic Particle Imaging

Magnetic particle imaging (MPI) should not be confused with MRI, as traditional MRI scanners cannot create an MPI image. The change in proton relaxation under the influence of SPIOs is observed as a contrast in MRI, while in MPI the signal originating from the SPIOs is directly detected. For the benefit of readers of molecular imaging, we will explain the MPI hardware and image acquisition in brief.

MPI hardware architecture consists of a pair of magnets forming the gradient field, slow shift magnets, and a pair of transceiver coils. A field-free region (FFR) in the form of a point or a line is created by bringing closer the "like" poles of two magnets. The magnetic field aligns to create a gradient, with the field at the center being close to nil (at UC Berkeley, 2.4 T/m and 7 T/m gradient fields were used). In MPI, the particles rotate only in the region of the FFR, while the particles outside the FFR remain saturated. The instantaneous location of the FFR allows for the spatial location of the signal in MPI. Slow-shift fields are generated by pairs of electromagnets that shift the field-free region in space. The slow-shift coil allows manipulation of the trajectory of FFR in space. The transceiver coil generates a sinusoidal radiofrequency oscillation (typically at 20 kHz at 20 mT in UC Berkeley scanners) that excites the SPIOs at the location of the FFR. SPIOs subsequently generate a signal that is picked up as induced e.m.f. in the receiver coil by Faraday's law of induction. For more information on MPI hardware, the readers can refer to other research articles [5, 62–69]. Different approaches are implemented to acquire MPI images. The system matrix is one of the first methods used for MPI image acquisition. In the system matrix, the harmonic response of particles to a sinusoidal excitation is calibrated in all possible locations in space [70, 71]. This forms the basis for the set. The MPI images are generated by solving a set of linear equations based on the calibrated system matrix. The x-space method of MPI image acquisition is shown in Figure 5. The x-space approach does not require precalibration; rather, the signal received is directly gridded to the spatial distribution of the SPIO tracer by knowledge of the instantaneous location of the field-free region (FFR), as shown in Figure 5 [66, 72, 73]. Several research articles and review articles have comprehensively explained the working, design, and imaging reconstruction in MPI scanners [11, 74–76].

Recently, efforts have been put into reconstructing MPI images using deep learning and convolutional neural network (CNN)-based methods. The classical inverse problem approach to image reconstruction is solved iteratively, requiring a harmonic basis set as in the system matrix approach that precalibrates the MPI system, which can be suboptimal in computational performance. A deep/machine learning approach using neural networks and training data could optimize MPI image reconstruction. Chae confirmed by training a single-layer network on MPI images that the spatial basis vectors of the MPI kernel are Chebyshev polynomials [77]. This key result was shown in classical MPI by Rahmer et al. [7] and Lu et al. [15], for system-matrix and x-space-based reconstruction methods, respectively. Subsequently, a multilayer CNN was used to show successful MPI image reconstruction from data generated using model-based simulation with tracers larger than 35 nm. Further investigations using deep image priors and comparisons between various regularization techniques in the context of MPI reconstruction as a constrained optimization problem have also been done by Dittmer et al. [78] and Askin et al. [79]. Shang et al. [80] utilized fusion dual-sampling by combining two neural network branches with and without a pooling layer to retain high-resolution information in the MPI image. This method was compared against other single-network CNNs to investigate resolution improvements. The above studies were done with the help of public MPI datasets such as OpenMPIData [81].

Classification of MPI data using artificial intelligence is also a burgeoning field. Identifying the region of interest (ROI) where the MPI tracer accumulates can be crucial for diagnosis and cell tracking. Manual identification of ROI is often time-consuming, and automatic segmentation of MPI images could quicken the diagnostic read. On these lines, Hayat et al. [82] used the K-means++ unsupervised learning algorithm to segment in-vivo rodent MPI images for localized iron quantification.

Newer MPI technologies, such as pulsed MPI and Color-MPI can measure the relaxation time constant of the iron

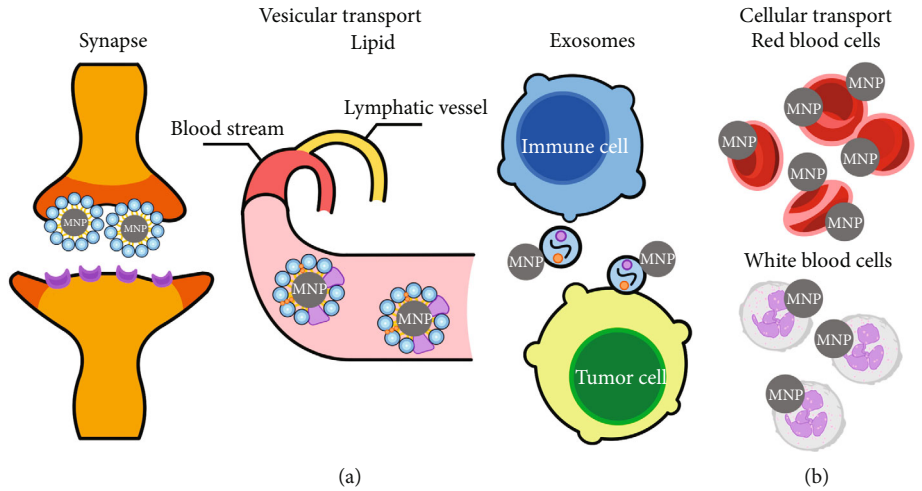

Figure 4: Vesicular transport is the predominant mechanism by which essential biomolecules are transported. (a) This consists of synaptic vesicles, lipid vesicles carrying fat, such as chylomicrons, and exosomes containing essential tumor markers. MPI, being a nonradioactive and nanoparticle-based tracer imaging modality with persistent signal *in vivo*, is ideally suited to study vesicular transport mechanisms to provide functional information. (b) MPI tracers can be safely used to label RBCs and WBCs and will soon play a pivotal role in cell-based immunotherapies (MNP: magnetic nanoparticles).

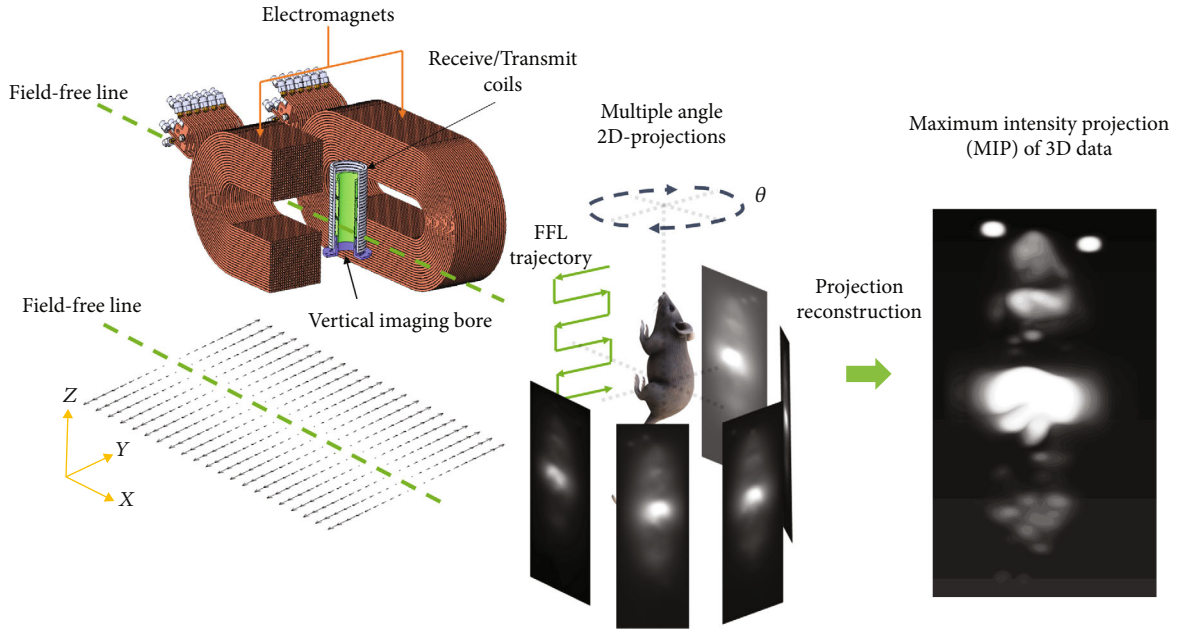

Figure 5: X-space MPI with a field-free line scanner. We illustrate the functioning of x-space MPI using a custom-built, vertical-bore 6.3 T/m field-free line (FFL) scanner. The FFL is created by a specialized iron return core electromagnet that serves as a slow-shift magnet as well. 2D-projection images are acquired by shifting the FFL in the *x-y* plane while translating the sample in the *z*-direction. In MPI, a time-varying field is applied, and only the particles at the FFL flip in response. The flip generates a signal in a receiver coil due to Faraday's law of induction and rastering the FFL allows the signal to be spatially localized. The MPI scanner allows for 2D projection and 3D tomographic imaging of the spatial distribution of superparamagnetic iron oxide nanoparticle tracers (SPIOs). Classical projection reconstruction algorithms can be implemented to reconstruct 3D MPI images from 2D projections [6, 11, 88]. Image reproduced under the Creative Common license CC-BY-4 from Chandrasekharan et al., Nanotheranostics, 2021 [23].

oxide nanoparticles and provide information about the local environment surrounding the particles influenced by the diseased physiology [52, 83–85]. This could be viscosity changes, temperature changes, or both [86, 87].

Both the SPIO tracers and MPI scanners have no ionizing radiation, and many tracers have already been approved by the FDA or EU as safe for human use [66, 89–91]. The SPIOs remain superparamagnetic until hydrolyzed or enzymatically degraded, as demonstrated by months-long longitudinal *in vivo* MPI cell tracking studies [33, 34, 92]. Injected SPIOs are typically cleared through the hepatobiliary system to reduce the renal burden [30]. MPI is extremely useful for

diagnosing pathology related to vascular changes and cell tracking. In the next few sections, we will discuss some of these key applications using MPI and their clinical translation.

4. MPI for Vascular Imaging

Changes in the vasculature of organs are a strong diagnostic indicator of organ damage. It is estimated that over eight million myocardial perfusion scans [93] and another 62 million CT angiograms are performed every year in the US [94]. In a typical perfusion scan, a tracer is injected as a bolus, and the signal (s(t) ∝ f (concentration of tracer), c(t)) as a function of time is captured using the imaging modality. The pattern of tracer uptake can be evaluated, and various tracer uptake parameters can be estimated. Tracer kinetic models are valuable in vascular perfusion-based diagnosis and treatment planning. MPI-based perfusion studies have been performed in preclinical murine models. Similar to tissue perfusion studies performed using ^{99m}Tc-sulfur colloids and RBC labeled with ^{111}In in scintigraphy, MPI has shown promise in diagnosing vessel-related pathology. MPI has a longer imaging window and superior SNR, but no radiation and no radioactive decay time constraints. MPI is also linearly quantitative, so tracer kinetic models that evaluate tissue perfusion parameters in scintigraphy can also be directly implemented in MPI. As shown in Figure 2, the SPIO tracers are comparable to sulfur colloids in size; however, the surface coating influences the circulation time and thus their use for vascular diagnosis. Carboxydextran-coated SPIO tracers, such as Vivotrax™ and Resovist, have a very short circulation time and are immediately taken up by the reticuloendothelial organs of the liver and spleen (Figure 6(a)). This form of biodistribution is similar to the tracers of ^{99m}Tc-sulfur colloid [95] and is useful for liver-spleen imaging. SPIOs with polyethylene glycol surface modification show better steric hindrance and avoid protein opsonization when administered intravenously, resulting in long circulation and a blood half-life of ~4.2 hours in rodents (Figures 6(b) and 6(c)).

Figure 6 illustrates the difference between polyethylene glycol (PEG)-coated long-circulating MPI tracers versus carboxydextran-coated MPI tracers of Ferucarbotran. The dextran-coated particles are readily taken up by the reticuloendothelial (RES) organs of the liver and spleen. While the PEG-coated particles resist opsonization and have a longer circulation time. MPI was useful in estimating the particle tracer kinetics. The signal from the major artery (ventricle of the heart) from a time series of data was fit to a monoexponential model ($s = s_0 \exp(-t/t_{1/2})$), where $t_{1/2}$ can be estimated by the knowledge of the signal of the tracer in the blood) to estimate the blood half-life of the tracer. PEG-coated particles from the LodeSpin lab have a blood circulation blood half-life of about 4.2 hours, while Ferucarbotran has a blood circulation blood half-life of about 0.17-0.5 h [20, 30, 96]. Using a similar approach and an inert coating of PEG-silane, the team at the University of Florida calculated the blood circulation half-life time for their tracers to be $t_{1/2} \sim 7$ hours [20].

Intravenously injected tracers partition within the plasma component of the blood. It is possible to achieve long blood circulation of the MPI tracer by encapsulating iron oxide nanoparticles within red blood cells (RBCs) [32, 97]. RBCs are e-nucleated and make up the largest component of the circulating blood cells. Similar to ^{99m}Tc-RBC and ^{111}In-RBC scintigraphy studies that are routinely performed to estimate myocardial perfusion, SPIO-labeled RBCs were used in evaluating cardiac function using a murine model. The group at Università degli Studi di Urbino subjected RBCs to a hypotonic solution containing ferrofluids. By doing so, the RBCs develop small pores that allowed movement of the SPIOs into the RBCs, and the RBCs reseal once the tonicity is restored [58]. The RBC-loaded MPI tracer had a 2- to 3-fold improved circulation half-life relative to bare SPIOs. The authors were able to observe the cardiac output and artifacts due to respiration using 3D MPI [32]. Using RBCs to encapsulate SPIOs for long circulation ensures biocompatibility. However, tradeoffs of this method include the need for routine quality checks that ensure the labeled RBCs are healthy and have low MPI sensitivity from MPI labeling. Therefore, researchers typically prefer commercially available long-circulating MPI tracers.

With zero background signal, MPI has an advantage over other modalities for imaging the vasculature. It has been known for decades that hemodynamic and metabolic changes are linked to neuronal activity, including cerebral blood flow (CBF), cerebral blood volume (CBV), and cerebral metabolic rate of oxygen ($CMRO_2$). These can be mapped quantitatively with optical, PET, and MR imaging. The hemodynamic response to brain activity is delayed by about 3–6 seconds [98]. These methods have weak sensitivity due to the low CBV signal: gray matter CBV is $5.2 \pm 1.4\%$ and white matter CBV is $2.7 \pm 0.6\%$ [99]. More recent MRI measurements show CBF increases roughly 3-fold more than $CMRO_2$ following brain activation [100]. CBV also shows strong changes (27%) after activation [101]. CBV changes are thought to better localize neuronal activity than CMRO2 [102–106].

The CBV change can be directly measured as a change in a signal using a long-circulating tracer in MPI, with an increase in signal resulting from the dilatory effect in the vessel. One of the first studies evaluating the neuronal response using MPI was done by a team at Massachusetts General Hospital [108]. The group developed a hand-held magnetic particle spectroscopy device (MPS) that detects the MPI tracer response based on the location at which the device is used for probing. Otherwise, the device does not provide any spatial information. Using long-circulating MPI tracers from Ocean Nanotech, the group noticed a remarkable change in the contrast-to-noise ratio (CNR) of fifty from changes in the CBV in the rodent's brain subjected to hypercapnia breathing. At UC Berkeley, using a field-free point scanner and long-circulating tracers of LodeSpin, the global CBV of a rodent brain was mapped with the difference in perfusion observed inside and outside the brain cortical regions (Figure 7). MPI has also been used to study ischemic as well as hemorrhagic strokes of the brain. The group from the University Medical Center Hamburg-Eppendorf

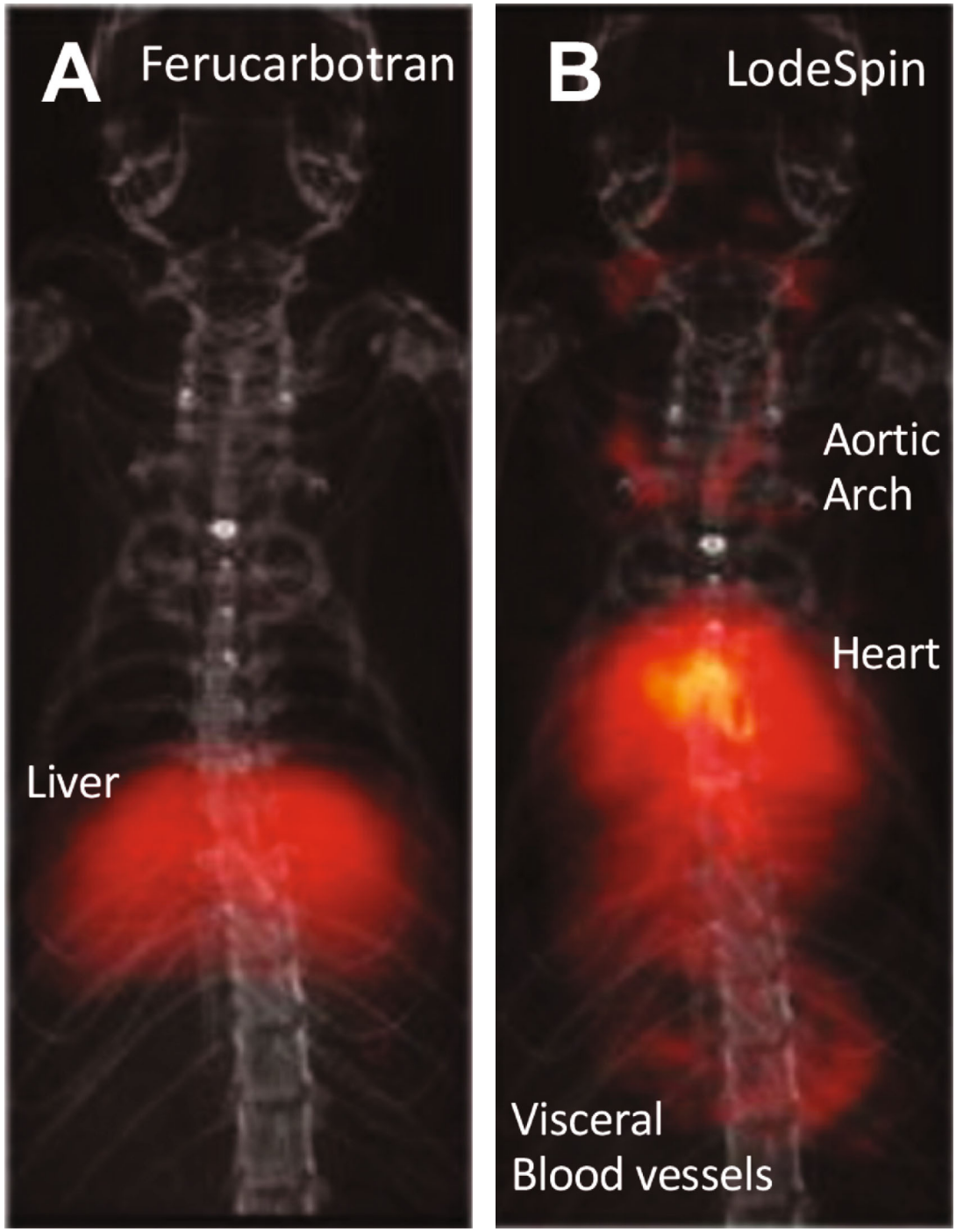

(a) (b)

Figure 6: Continued.

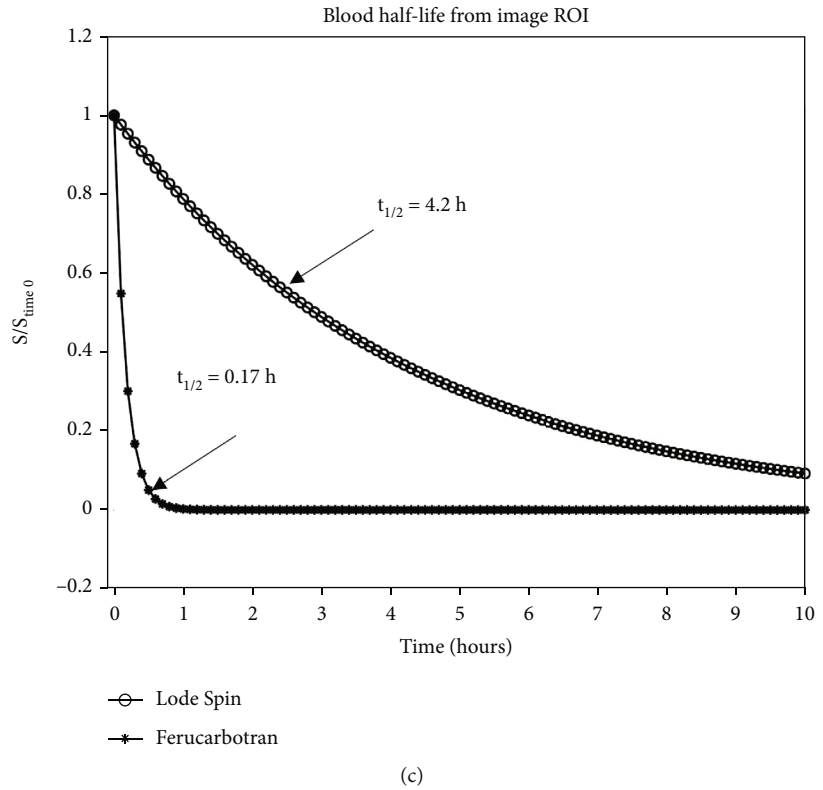

(c)

Figure 6: MPI studies are comparable to ^{99m}Tc-sulfur colloids and ^{111}In RBC scintigraphy studies. (a, b) MPI images overlaid on an X-ray CT image for anatomical reference at 10 minutes post i.v. administration of carboxydextran-coated SPIO, Ferucarbotran, and polyethylene glycol (PEG)-coated long-circulating SPIO of LodeSpin, respectively. Ferucarbotran has a shorter blood half-life and is rapidly taken up by the liver, similar to sulfur colloid tracers (c). On the other hand, PEG-coated SPIOs show a longer blood circulation time of about 4.2 hours and are useful in perfusion studies similar to ^{111}Inlabeled red blood cell scintigraphy but without any radiation. (Image reproduced with permission from Kesleman et al., Phys Med Biol. 2017) [30].

acquired MPI images at forty-six volumes per second, enabling the first-pass tracer perfusion measurements in a rodent model of mid-cerebral arterial occlusion [109]. The first-pass measurement allowed for the diagnostic evaluation of kinetic parameters, including the tracer transit time, CBF, and CBV. In a similar approach, the same group also used MPI to evaluate cerebral hemorrhages as well [110]. Determining hemorrhagic versus ischemic stroke is crucial in defining the course of treatment.

At UC Berkeley, we evaluated the CBV changes in a rodent model of traumatic brain injury (TBI) [28]. This was one of the first studies to visualize the primary brain injury and associated hematoma in TBI using MPI. The MPI data showed the severity, and depth of TBI-associated vascular damage. The work also showed immune-related activity as a sign of the repair mechanism of the brain-related injury [28].

Once again, MPI complements imaging techniques in nuclear medicine. MPI tracers involve no complex radiochemistry and can be stored and used without prior preparation. Some of the kinetic models that are used in scintigraphy and PET can be directly adapted for MPI.

Gastrointestinal (GI) bleeding in humans is caused by various conditions, including trauma to the lower abdomen, due to inflammation, carcinoma, and Meckel diverticulum (where the intestinal wall folds itself) [111, 112]. Though the bleed onset can be asymptomatic, it can range in severity from acute to chronic to obscure and can occur anywhere in the lower and upper parts of the GI tract. The first UC Berkeley publication detected GI bleeding using 2D projections, similar to projection scintigraphy, in a murine model of familial adenomatous polyposis (FAP) [27] [113]. Apc^{Min} (min, multiple intestinal neoplasia) is a point mutation in the murine homolog of the adenomatous polyposis coli (APC) gene [99]. This mutation is often found in patients with FAP, a hereditary form of colon cancer. Polyps spontaneously develop in these mice with age, causing bleeding and anemia [114].

We induced acute bleeds by administering an anticoagulant (heparin) and tracked the bleed with MPI (Figure 8). Using an irreversible tracer kinetic model or classically referred to as the Patlak model, allowed for bleed rate estimation. Using MPI, we observed a sensitivity of 1-5 μl/min blood volume which was 10 times more sensitive than RBC scintigraphy.

MPI is uniquely suited for imaging the lungs, as it is not affected by depth limits or air-tissue-related susceptibility effects. Pulmonary embolisms (PE) have a 30% mortality rate when left untreated, but the mortality rate improves to 8% after emergency treatment.

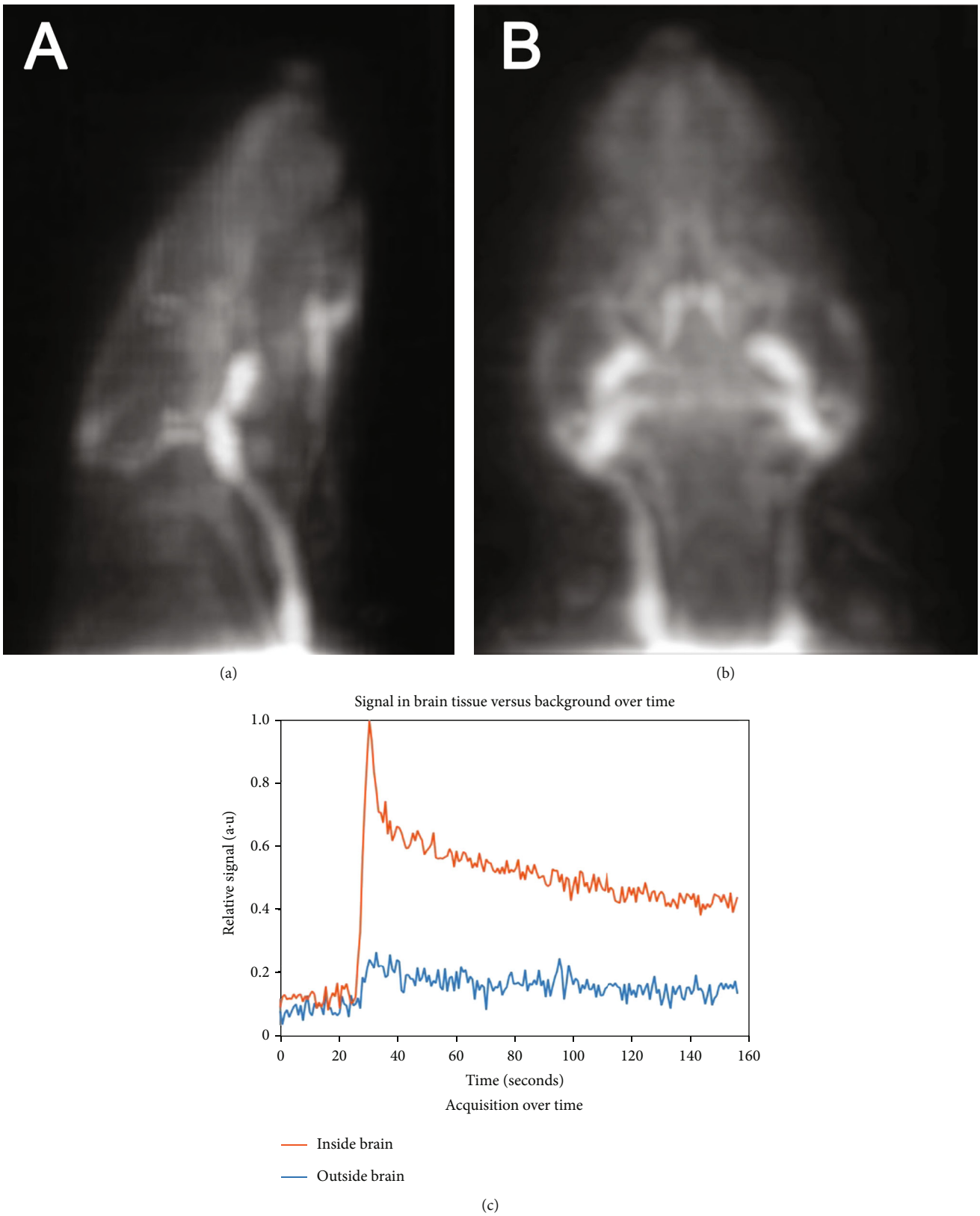

Figure 7: Functional brain imaging. MPI images of whole brain blood volume (a, b) were imaged using a long-circulation tracer. (c) The tracer kinetics measured using MPI show a wash-in phase and a wash-out phase from the region of interest (ROI) within the brain, while the signal change in the background is negligible [28]. MPI CNR is ideal for functional brain studies, as MPI shows no obscuring background [1, 107].

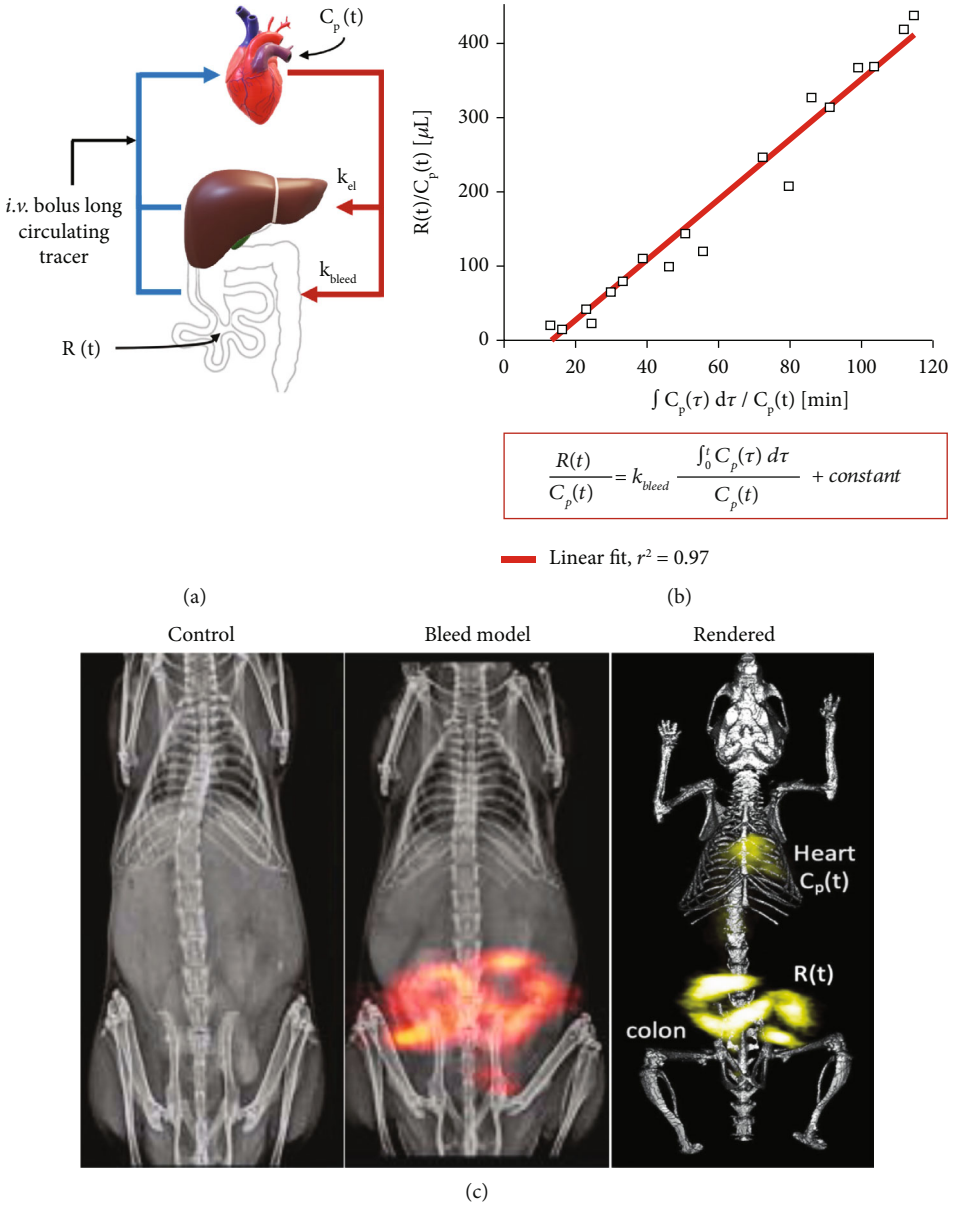

FIGURE 8: Kinetic models from scintigraphy and PET studies can be directly adopted for use with MPI. The most common model of irreversible tracer uptake or the Patlak model was used to quantify the rate of gut (GI tract) bleeding using MPI in a murine model. The approach assumes (a) a central compartment consisting of the tracers in the circulation from which $C_p(t)$ can be calculated from the MPI signal from the ventricle of the heart and a peripheral compartment in which the tracer enters irreversibly at the rate constant k_{bleed}. (b) The slope of the rate equation from the graph can be used to estimate the rate of bleeding. (c) Dynamic MPI images show the central compartment (heart) and the peripheral bleed compartment (GI tract) (MPI images are overlayed on X-ray projection data (grayscale) for anatomical reference). (Adapted with permission from Yu et al., ACS Nano, 2017. Copyright (2017) American Chemical Society) [27].

The emergency diagnosis of PE is challenging due to nonspecific symptoms, such as chest pain and/or shortness of breath. Many cases of PE are only diagnosed postmortem [115]. Hence, the imaging studies CT pulmonary angiography (CTPA) and ventilation/perfusion scintigraphy (V/Q) are crucial for the definitive diagnosis of PE. Because the V/Q exam is slow (3 hours) and provides poor spatial resolution (5 mm) [116–118], CTPA has become the gold standard PE diagnostic imaging method [116, 119]. Two large subpopulations—patients sensitive to iodine contrast and pregnant patients—cannot tolerate CTPA, and hence these patients undergo V/Q. However, V/Q's total exam time (3 hours) is too slow to provide an emergency diagnosis. MPI, on the contrary, could provide a rapid, zero-radiation complement to V/Q [120]. At UC Berkeley, we conducted the first-in-animal ventilation/perfusion MPI studies, surpassing the dose-limited sensitivity of nuclear medicine [24, 31] (Figure 9).

Since MPI tracers have no radioactive half-life, they can be prepared and stored in the refrigerator. SPIOs coated with macroaggregated albumin (MAA) could be injected directly from the refrigerator, and an emergency MPI scan can be

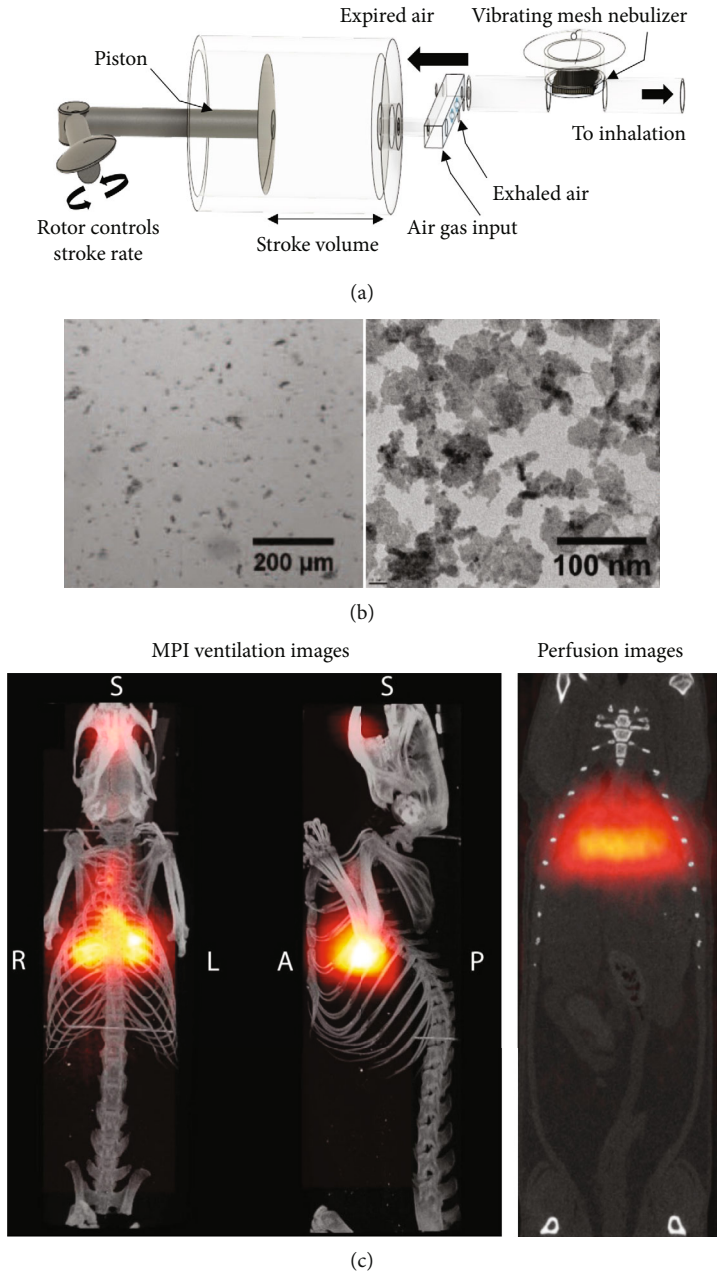

Figure 9: Lung ventilation/perfusion studies using magnetic particle imaging. (a) An Engineered mechanical ventilation device with a vibrating mesh nanoparticle aerosolizer for ventilation study of the lungs using MPI. (b) SPIOs aggregated in macroaggregated albumin (MAA) for lung perfusion studies. (c) MPI lung ventilation/perfusion images co-registered with X-ray images as an anatomical reference [24, 31] (reproduced with permission from IOP Publishing and under the Creative Common license).

done in just a few minutes. This is much faster than the traditional ^{99m}Tc-MAA studies with scintigraphy or SPECT, which typically requires three hours. Newer MPI approaches exploit a doppler-like effect from the magnetic nanoparticles to measure blood flow velocity [121], which can minimize certain imaging artifacts in MPI.

5. MPI for Cell Tracking and Immunotherapy

MPI is uniquely suited for tracking therapeutic and diagnostic cells *in vivo*. With a growing number of cell-based therapeutics, there is a particular need to validate and follow such therapies and be able to provide information on the treatment progress. Therapies based on stem cells and therapeutic immune cells such as chimeric antigen receptor (CAR) T cells, tumor-infiltrating lymphocytes (TILs), and CAR-NK cells have shown promising treatment outcomes for treating cancer, inflammation, and various degenerative diseases.

MPI tracers are biodegradable and nonradioactive. In the previous section, we showed that tracers of MPI can be packaged into RBCs and can be used as a blood-pool agent like ^{99m}Tc-RBCs. However, encapsulating nucleated cells such as lymphocytes using radioactive isotopes like ^{99m}Tc and ^{111}In have a debilitating effect on the cells. Labeling cells

with ^{111}In could lead to chromosomal aberration, cell death, and ultimately cell dysfunction [122, 123]. Cells labeled with ^{111}In can be exposed to as much as 90 Gy radiation per 10^8 cells [124]; whereas, the iron oxide nanoparticles used for MPI are readily taken up by cells and are nontoxic to the labeled cells.

When it comes to regenerative cell therapies like stem cell therapy, certain posttherapy observations can be of immense diagnostic importance, including (a) observing if the implanted stem cell is growing and differentiating into the desired cell type, (b) determining whether or not the implanted cells are alive, and (c) understanding the fundamental biodistribution (ADME) of the introduced stem cells [125, 126].

MPI has by far the highest sensitivity for cell tracking (~200 cell sensitivity) [1, 34]. One of the first stem cell "hot spot" imaging was reported in the year of 2015 [35]. Bulte et al. implanted SPIO-labeled mesenchymal stem cells (MSCs) using a stereotaxic setup into the striatum of a rodent brain. The authors reported the possibility to track 50,000 labeled stem cells. At UC Berkeley, long-term tracking of SPIO-labeled neuronal progenitor cells was carried out by the stereotaxic introduction of labeled cells in the brain [34]. In this work, an incredible 5 ng/voxel (~200 cell detection limit) was reported using a 2.3 T/m gradient MPI scanner. Further, MPI tracked cells for ~87 days with no loss of tracer signal. In another approach, MSCs labeled with SPIO were injected intravenously and tracked using MPI (ADME) [34]. The injected cells were tracked to the lungs of the rodent, which they initially traverse due to the physiology of the vascular system, followed by clearance of labeled cells to the liver and spleen. These studies show that the MPI can track the biodistribution of injected therapeutic cells with superb sensitivity. In another collaborative research from Harvard and Michigan State University, researchers labeled islet cells with SPIOs and tracked the islet cell graft in a rodent model using MPI. MPI provided high contrast in imaging insulin-expressing graft cells [127]. Researchers have also covalidated stem cell tracking using bi- and trimodal approaches and compared it with that of MPI [22, 128, 129]. Multimodal imaging complements the strengths of each modality and improves the overall diagnosis.

Cancer prognosis and its response to immunotherapy depend on the tumor microenvironment. For instance, the tumor burden of immune cells, such as the CD4/CD8 T cells, can predict the tumor response to checkpoint immunotherapy [130, 131]. The immune-rich tumor microenvironment can have a favorable outcome in treating cancer with immunotherapy [132]; whereas, a tumor-rich microenvironment with inflammatory cells of neutrophils and macrophages can cause tumor metastasis [133–135]. MPI was utilized to assess the tumor microenvironment.

Nanoparticles have been shown to accumulate in tumor lesions through a process of enhanced permeation and retention (EPR). EPR occurs because of leaky vasculature resulting from uncontrolled angiogenesis happening within a tumor. As a result, macromolecules like albumin and injected nanoparticles from blood plasma accumulate within the tumor milieu and are retained. At UC Berkeley, we observed EPR for the first time using MPI. Using a xenograft cancer model of triple-negative breast cancer in a rodent, i.v.-injected long-circulating tracers of LodeSpin showed classical rim enhancement of the tumor at earlier time points followed by core enhancement at later time points, with peak tracer signal observed in the tumor at 6 hours posttracer administration (Figure 10(a)) [38]. Histology from the study showed a strong correlation between immune cell uptake within the tumor and that of the MPI tracers (Figure 10(b)).

In a follow-up study, researchers from Western University and Michigan State University used MPI tracers of ferucarbotran and ferumoxytol to label the monocytes of the liver and spleen;these in situ labeled immune cells then infiltrated a highly metastatic breast cancer xenograft of 4 T1 in a murine model [37] and were observed using MPI. The authors shed new light on the EPR phenomenon using MPI. The current work and recent studies on EPR suggest that beyond the leakiness of the tumor vessels, the uptake of nanoparticles by the immune cells and the tumor microenvironment can all contribute to the EPR effect. Immune cells, such as macrophages and neutrophils, are involved in cancer metastasis, and tracking tumor-associated macrophages (TAMs) and neutrophils (TANs) is of immense diagnostic and therapeutic value. Furthermore, imaging the EPR effect using MPI can be a helpful indicator for classifying responders and nonresponders to nanotherapeutics [136]. In a similar approach, a group at Stanford labeled macrophages *in vitro* and tracked them toward sites of neuroinflammation in a murine model [59].

White blood cell (WBC) scans are often used to diagnose inflammation and fevers of unknown origin (FUO). By radiolabeling and tracking autologous immune cells, radiologists can visualize areas of high immune activity that highlight pathologies, such as inflammation, infection, or cancer. Antibodies are biomolecules that can bind to a molecular target with very high specificity. Antibodies functionalized with radioisotopes are used to track and identify the overexpression of molecular targets using PET/SPECT, thereby providing spatial information on biomolecule expression, for instance in cancer. In a molecular imaging approach at UC Berkeley, we utilized SPIOs functionalized with antibodies (anti-Ly6G) that are specific towards antigens expressed on the surface of inflammatory cells of neutrophils and macrophages, which allowed us to label them in situ in a mouse model and track them towards sites of bacterial lipopolysaccharide (LPS)-induced acute inflammation (Figure 11) [23].

In a healthy mouse, i.v.-injected IgG-based antibody-MPI tracers are distributed in the bone marrows of the skull, limbs, pelvic bones, and the RES organs of the spleen and liver. In addition, the antibody-MPI tracers also accumulated in the renal organs (Figure 11(a)). This observation is critical for antibody-MPI and indicates preserved antibody function. This is because MPI tracers without antibodies are mostly cleared via the hepatobiliary route rather than the renal route.

The anti-Ly6G antibody MPI tracer was injected into a mouse model of LPS-induced myositis, and the tracer was distributed to the inflammatory site compared to the

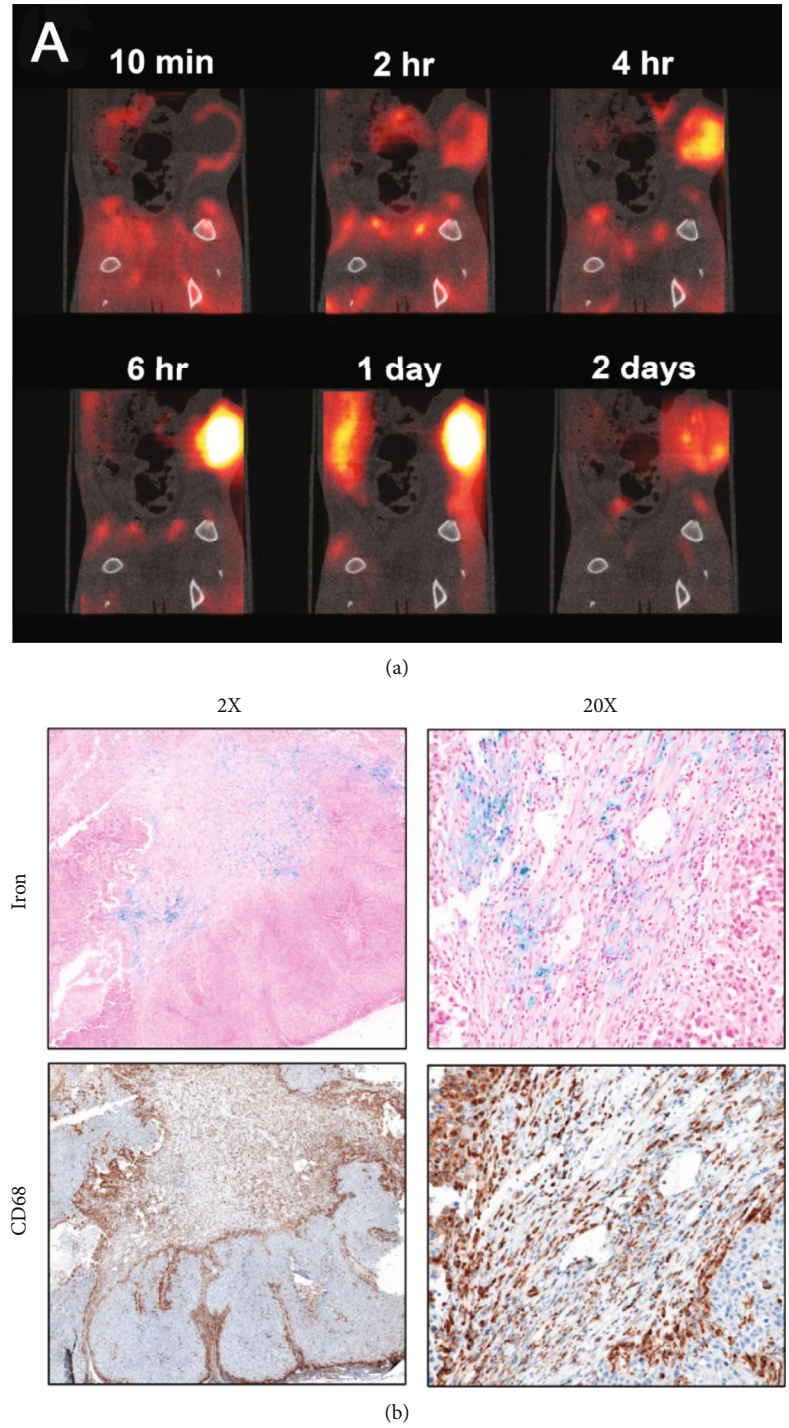

Figure 10: UC Berkeley MPI images show the EPR effect in breast cancer (MDA-MB231) tumor model in an athymic rat [38] (a) Tracer dynamics: rim enhancement followed by EPR and cellular uptake and washout. (MPI images are coregistered with X-ray images for anatomical reference.) (Adapted with permission from Yu et al., Nano Letters, 2017. Copyright (2017) American Chemical Society [38]) (b) Iron and rat macrophage colocalization histology: side-by-side comparison of identical tissue sections stained with Prussian blue and CD68 shows iron-laden macrophages (blue) present in the central stroma of the xenograft that is positive for macrophage marker CD68 (brown).

contralateral side. The antibody binds to specific cell surface markers on inflammatory cells of neutrophils (Ly6G in this case), and the tracer-bound inflammatory cells home into the sites of myositis, providing a means to diagnose infection, inflammation, and possibly cancer [23, 137, 138].

Antibodies used as therapeutics have a complex biodistribution and elimination pattern. The monoclonal antibody of IgG can have a long blood-half life or bind to their targets and clear rapidly. Radiolabeled IgGs have shown initial biodistribution into the hepatobiliary organ,

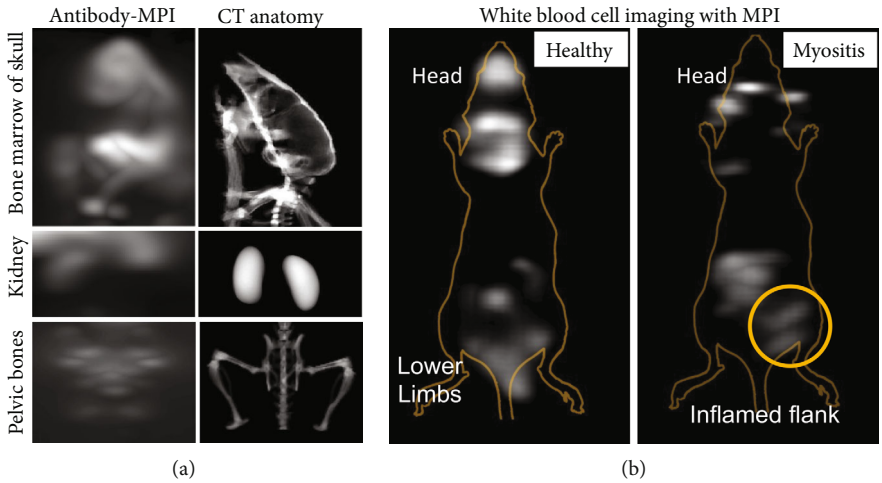

Figure 11: (a) Maximum intensity projection (MIP) of 3D MPI using anti-Ly6G antibody SPIOs (neutrophil targeting) compared to an X-ray CT image of a mouse. The antibody tracers of MPI are distributed in bone marrow of the skull, limbs, pelvic bones, and reticuloendothelial organs of the liver and spleen. The antibody tracers also accumulate in the kidneys. This clearance pattern is observed in antibody-based therapeutics, which is atypical for MPI tracers to accumulate in the kidneys [3, 148]. MPI can thus be tremendously valuable for tracking antibody therapeutics with negligible renal toxicity, often observed in radioactive antibody tracers. (b) Anti-Ly6G antibody MPI tracer imaging of inflammation/infection in a murine model of bacterial myositis using lipopolysaccharide (LPS) on the right flank. MPI showed a CNR of ~8-12 in the inflammatory site versus the contralateral side (data overlayed on a mouse anatomical outline, with the liver signal segmented through apodization) [23, 138, 148].

organs of the RES, lungs, GI tract, and kidneys [139], but their elimination route seems to depend on various factors. For example, small-size proteins and antibody fragments are cleared via the renal route, whereas larger-size antibodies are removed via the hepatobiliary route [140]. Further, nontargeted uptake of antibodies can occur differently based on the radioactive element bound to the antibody [141, 142]. The catabolized fragments of radiolabeled antibodies have been shown to pose a radiation risk to renal organs [143].

As a nonradioactive tracer imaging modality, MPI can be used to track antibody-nanoparticle conjugates with no harm to the off-target sites of tracer accumulation. However, we need to be cautious of the size of the antibody-nanoparticle conjugate that could impede the antibody function. In the study using the anti-Ly6G antibody described above, the molecular targets were present in the circulation, and it did not need to cross the vascular endothelium. More research along the transport mechanism of the antibody-SPIO conjugate could shed light on the molecular mechanism and enable future molecular imaging approaches using MPI. Nevertheless, IgMs, a pentamer of IgG with superior avidity, are around ~20 nm. This is close to the size of the nanoparticles used as MPI tracers and can bind to molecular targets. By carefully engineering antibody-MPI tracer conjugates, we can achieve nanoparticle delivery across vascular endothelium using antibody-SPIO and provide a means for molecular imaging using MPI.

Researchers at Beihang University and the Chinese Academy of Sciences extended the study above with antibodies to evaluate NETosis in lupus, an autoimmune condition that can become fatal to the patient overtime. The authors showed that using MPI and anti-Ly6G-SPIOs, neutrophils infiltrated the lung peritoneum due to a lupus-based inflammatory response [144]. Antibody-MPI can be further extended towards understanding the cancer microenvironment using tracers targeting CD4 and CD8 T cell subtypes and can also be exploited for imaging antibody-based immunotherapies [145].

Another area of immense interest is the noninvasive tracking of chimeric antigen receptor (CAR)-based immunotherapies and the treatment response. Chimeric antigen receptors are also specific to a molecular target, like antibodies. However, once the CAR binds to the molecular target, it can trigger a kill switch in the CAR-carrying T or NK cells. Interest in tracking adoptively transferred T cells began in the 1980s. Researchers have used ^{111}Inlabeled tumor-infiltrating lymphocytes (TILs) to determine cell localization in tumor lesions [146, 147]. However, as pointed out by the authors in the study and as discussed earlier, radiation exposure to lymphocytes such as T cells, B cells, and NK cells impedes their functions and causes cell death. Immunotherapy using CAR cells and TILs sometime require weeks to even months to see any appreciable response from the tumor.

Immunotherapy response evaluation criteria, such as the Lugano criteria and the Olsen criteria are designed for monitoring the response in blood tumors to treatment (e.g., lymphoma) [149, 150]. Activities such as nodal swelling, activity in reticuloendothelial organs, and signs of inflammation are often monitored. These activities do not directly indicate the activity of the drug (antibody or CAR-T cells). MPI, for this reason, is uniquely suited for tracking CAR and TIL-based immunotherapy, since the MPI signal persists for a long time and the tracers are not toxic to the labeled cells. Thus,

MPI allows for real-time spatial localization of the CAR-labeled cells and provides treatment insights to the oncologists, allowing them to optimize immunotherapy for each patient. Further, it can provide information on whether the administered CAR-Ts are dead or alive and active [86].

For example, the team at the University of Florida was successful in labeling T cells specific to the PMEL marker on brain tumor cells using SPIOs and tracking them toward aggressive tumors of glioma in a murine model [36]. In another approach, researchers at Stanford labeled CAR-T cells specific to the cancer checkpoint marker B7-H3 using a mechanoporation approach and successfully tracked the labeled cells to a tumor xenograft using a multimodal imaging approach encompassing MPI, MRI, and photoacoustic imaging [151].

MPI can be utilized for precision and personalized immunotherapy tracking. CAR-based immunotherapy with increased target specificity, for example, using a synNotch transcriptional circuit, is an approach to recognize multiantigen priming and target-specific killing of cancer cells that can also be repurposed for early diagnosis of cancer [152]. Using multiple priming targets that are expressed in the early stages of cancer, one can implement MPI and track engineered T-cells to recognize tumors at an early stage, providing a means of early-stage cancer screening. Immunotheranostics using MPI can be useful for the early diagnosis of a myriad of immune-related disorders.

In a separate review, we have further detailed the use of magnetic particle imaging exclusively for cancer theranostics [39, 153].

6. MPI in Metabolic Imaging

Since MPI tracers are "nano" in scale and dimension, MPI cannot mimic small molecule imaging in PET and SPECT. However, MPI can track tracers encapsulated within synaptic vesicles of neurons, fatty acid vesicles of chylomicrons, and functional vesicles of exosomes (Figure 4).

Exosomes, a form of extracellular vesicles (EV) that contain protein and other macromolecular constituents, are excreted from cells and carry pertinent information about the cells [60]. The group from Stanford exposed cancer cells to anaerobic conditions and radiation exposure to generate exosomes that are readily taken up by cancer cells, but only under hypoxic conditions. Seventy to ninety percent of the exosomes were taken up by hypoxic cancer cells but not by cancer cells exposed to aerobic conditions. The exosomes of 50 -200 nm sizes were readily labeled with MPI tracers and showed an antitumor effect in a xenograft murine cancer model in vivo.

Chylomicrons are small fatty vesicles and play a role in fat metabolism and fat transportation across various tissues. Brown adipose tissue (BAT) has been demonstrated to regulate fat/glucose metabolism and body temperature. During the activation of BAT, chylomicrons transport triglycerides. They are also a major site for postprandial triglyceride clearance. The authors from Rheinische Friedrich-Wilhelms-Universität Bonn and Physikalisch-Technische Bundesanstalt developed artificial chylomicrons containing triglycerides and MPI tracers and showed that MPI could track BAT activation in a mouse model exposed to cold temperatures [26]. The cold exposure increases the BAT metabolism and thus the triglyceride consumption, resulting in a superior MPI contrast of the interscapular BAT tissue compared to that in the healthy control mouse.

In another interesting study, the team from the Chinese Academy of Science developed a surface-modified SPIO with 5-hydroxytryptamine (5-HT) that is oligomerized by the enzyme myeloperoxidase activity (MPO) expressed by neutrophils during inflammation [154]. The authors reported that the 5-HT tracers showed increased activity at inflammatory sites in a mouse model of vulnerable atherosclerotic plaque using MPI. The authors validated their findings using a multimodal imaging approach.

On a different note, the group at Michigan State University coencapsulated a therapeutic drug and SPIO within a polymer nanoparticle. Using MPI, they were able to quantify the amount of drug released from the particles [155]. The approach could be invaluable for controlling drug release and reducing chemotherapy-related toxicity.

MPI has also been explored for studying plants. Chelated iron fertilizers are used to evaluate chlorosis and damage due to reactive oxygen species production. Most of these studies rely on destructive spectroscopy techniques to probe plant elemental iron distribution. The team from Case Western formulated MPI tracers of different sizes in EDTA-based metal chelators and grew Lepidium sativum with roots soaked in water containing the iron formulation [156]. The authors showed that the nanoparticle formulation had greater uptake by the plants, resulting in enhanced biomass and chlorophyll production. MPI tracked the chelated nanoparticles in the plant system with minimal and nondestructive preparation of plant specimens.

7. Conclusion

In this review article, we have discussed how magnetic particle imaging (MPI), a new and radiation-free imaging modality, can complement nuclear medicine. Clinicians can directly adapt diagnostic approaches with colloidal tracers in scintigraphy for MPI but without any radiation. One can also readily repurpose existing tracer uptake kinetic models for MPI, such as for estimating the GI bleed using long-circulating tracers. MPI is unique because its tracer physics influence image resolution and sensitivity. Many MPI tracers are clinically available, and new ones with better MPI performance are being developed. Recently, we reported a new particle physics called superferromagnetism (SFMIO) that shows a 10-fold boost in resolution in MPI. Research along with new tracer development and biocompartmentalization with reduced toxicity can pave for clinical studies using MPI. MPI is uniquely suited for tracking cell-based therapies with zero radiation and no cell harm from labeling. Many research groups across the globe are pushing MPI towards the clinic with newer scanning approaches, lower magnetic gradients with reduced power requirements [157], cheaper one-sided MPI scanners [158], and safer RF [88].

Abbreviations

MPI: Magnetic particle imaging
SPIO: Superparamagnetic iron-oxide nanoparticles
CT: Computed tomography
MRI: Magnetic resonance imaging
FFR: Field-free-region
FFL: Field-free line
FOV: Field-of-view
PSF: Point-spread-function
MNP: Magnetic nanoparticles

Conflicts of Interest

Professor Conolly is a cofounder of an MPI startup company and Magnetic Insight, and he holds stock in this company. Dr. Goodwill is the CEO/CTO of Magnetic Insight.

Acknowledgments

The authors acknowledge support from the following sources: NIH grant R01s EB024578, EB029822, T32 GM 098218, and R44: EB029877; UC TRDRP grant 26IP-0049; UC Discovery Award; M. Cook Chair; Bakar Fellowship; NSERC PGSD Fellowship; UCB Bioengineering Craven Fellowship; UC CRCC Doctoral Fellowship; Siebel Scholars Program; and NSF GRFP.

References

[1] P. Chandrasekharan, Z. W. Tay, X. Y. Zhou et al., "A Perspective on a Rapid and Radiation-Free Tracer Imaging Modality, Magnetic Particle Imaging, with Promise for Clinical Translation," *The British Journal of Radiology*, vol. 91, no. 1091, article 20180326, 2018.

[2] X. Y. Zhou, Z. W. Tay, P. Chandrasekharan et al., "Magnetic particle imaging for radiation-free, sensitive and high-contrast vascular imaging and cell tracking," *Current Opinion in Chemical Biology*, vol. 45, pp. 131–138, 2018.

[3] P. Chandrasekharan, Z. W. Tay, X. Y. Zhou et al., "Chapter 15 - magnetic particle imaging for vascular, cellular and molecular imaging," in *Molecular Imaging*, B. D. Ross and S. S. Gambhir, Eds., pp. 265–282, Academic Press, 2021.

[4] E. U. Saritas, P. W. Goodwill, L. R. Croft et al., "Magnetic particle imaging (MPI) for NMR and MRI researchers," *Journal of Magnetic Resonance*, vol. 229, pp. 116–126, 2013.

[5] B. Gleich and J. Weizenecker, "Tomographic imaging using the nonlinear response of magnetic particles," *Nature*, vol. 435, no. 7046, pp. 1214–1217, 2005.

[6] P. W. Goodwill and S. M. Conolly, "The x-space formulation of the magnetic particle imaging process: 1D signal, resolution, bandwidth, SNR, SAR, and magnetostimulation," *IEEE Transactions on Medical Imaging*, vol. 29, no. 11, pp. 1851–1859, 2010.

[7] J. Rahmer, J. Weizenecker, B. Gleich, and J. Borgert, "Signal encoding in magnetic particle imaging: properties of the system function," *BMC Medical Imaging*, vol. 9, no. 1, p. 4, 2009.

[8] J. Franke, U. Heinen, H. Lehr et al., "System characterization of a highly integrated preclinical hybrid MPI-MRI scanner," *IEEE transactions on medical imaging.*, vol. 35, no. 9, pp. 1993–2004, 2016.

[9] T. Knopp, N. Gdaniec, and M. Moddel, "Magnetic particle imaging: from proof of principle to preclinical applications," *Physics in Medicine and Biology*, vol. 62, no. 14, pp. R124–R178, 2017.

[10] T. Knopp and A. Weber, "Sparse reconstruction of the magnetic particle imaging system matrix," *IEEE Transactions on Medical Imaging*, vol. 32, no. 8, pp. 1473–1480, 2013.

[11] J. J. Konkle, P. W. Goodwill, O. M. Carrasco-Zevallos, and S. M. Conolly, "Projection reconstruction magnetic particle imaging," *IEEE Transactions on Medical Imaging*, vol. 32, no. 2, pp. 338–347, 2013.

[12] M. Grüttner, T. Knopp, J. Franke et al., "On the formulation of the image reconstruction problem in magnetic particle imaging," *Biomedizinische Technik/Biomedical Engineering*, vol. 58, no. 6, pp. 583–591, 2013.

[13] D. A. Price, G. L. G. Sun, P. W. Goodwill, E. U. Saritas, and S. M. Conolly, "Improving conspicuity in MPI by equalization of the "broad tails" of the MPI point spread function," in *2013 International Workshop on Magnetic Particle Imaging (IWMPI)*, Berkeley, CA, USA, 2013.

[14] K. Lu, P. Goodwill, B. Zheng, and S. Conolly, "Multi-channel acquisition for isotropic resolution in magnetic particle imaging," *IEEE Transactions on Medical Imaging*, vol. 37, no. 9, pp. 1989–1998, 2018.

[15] K. Lu, P. W. Goodwill, E. U. Saritas, B. Zheng, and S. M. Conolly, "Linearity and shift invariance for quantitative magnetic particle imaging," *IEEE Transactions on Medical Imaging*, vol. 32, no. 9, pp. 1565–1575, 2013.

[16] R. M. Ferguson, A. P. Khandhar, S. J. Kemp et al., "Magnetic particle imaging with tailored iron oxide nanoparticle tracers," *IEEE Transactions on Medical Imaging*, vol. 34, no. 5, pp. 1077–1084, 2015.

[17] R. Hufschmid, H. Arami, R. M. Ferguson et al., "Synthesis of phase-pure and monodisperse iron oxide nanoparticles by thermal decomposition," *Nanoscale*, vol. 7, no. 25, pp. 11142–11154, 2015.

[18] L. M. Bauer, S. F. Situ, M. A. Griswold, and A. C. S. Samia, "Magnetic particle imaging tracers: state-of-the-art and future directions," *The Journal of Physical Chemistry Letters*, vol. 6, no. 13, pp. 2509–2517, 2015.

[19] L. M. Bauer, S. F. Situ, M. A. Griswold, and A. C. S. Samia, "High-performance iron oxide nanoparticles for magnetic particle imaging – guided hyperthermia (hMPI)," *Nanoscale*, vol. 8, no. 24, pp. 12162–12169, 2016.

[20] S. Liu, A. Chiu-Lam, A. Rivera-Rodriguez et al., "Long circulating tracer tailored for magnetic particle imaging," *Nanotheranostics*, vol. 5, pp. 348–361, 2021.

[21] L. Gloag, M. Mehdipour, M. Ulanova et al., "Zero valent iron core–iron oxide shell nanoparticles as small magnetic particle imaging tracers," *Chemical Communications*, vol. 56, no. 24, pp. 3504–3507, 2020.

[22] G. Song, M. Chen, Y. Zhang et al., "Janus iron oxides @ semiconducting polymer nanoparticle tracer for cell tracking by magnetic particle imaging," *Nano Letters*, vol. 18, no. 1, pp. 182–189, 2018.

[23] P. Chandrasekharan, K. L. B. Fung, X. Y. Zhou et al., "Non-radioactive and sensitive tracking of neutrophils towards inflammation using antibody functionalized magnetic particle imaging tracers," *Nanotheranostics*, vol. 5, pp. 240–255, 2021.

[24] Z. W. Tay, P. Chandrasekharan, X. Y. Zhou, E. Yu, B. Zheng, and S. Conolly, "In vivo tracking and quantification of

inhaled aerosol using magnetic particle imaging towards inhaled therapeutic monitoring," *Theranostics*, vol. 8, no. 13, pp. 3676–3687, 2018.

[25] K. Murase, M. Aoki, N. Banura et al., "Usefulness of magnetic particle imaging for predicting the therapeutic effect of magnetic hyperthermia," *Open Journal of Medical Imaging*, vol. 5, no. 2, pp. 85–99, 2015.

[26] S. Hildebrand, N. Löwa, H. Paysen et al., "Quantification of lipoprotein uptake in vivo using magnetic particle imaging and spectroscopy," *ACS Nano*, vol. 15, no. 1, pp. 434–446, 2021.

[27] E. Y. Yu, P. Chandrasekharan, R. Berzon et al., "Magnetic particle imaging for highly sensitive, quantitative, and safe in vivo gut bleed detection in a murine model," *ACS Nano*, vol. 11, no. 12, pp. 12067–12076, 2017.

[28] R. Orendorff, A. J. Peck, B. Zheng et al., "First in vivo traumatic brain injury imaging via magnetic particle imaging," *Physics in Medicine & Biology*, vol. 62, no. 9, pp. 3501–3509, 2017.

[29] K. Murase, K. Nishimoto, A. Mimura, M. Aoki, K. Hamakawa, and N. Banura, "Application of magnetic particle imaging to pulmonary imaging using nebulized magnetic nanoparticles: Phantom and small animal experiments," in *2015 5th International Workshop on Magnetic Particle Imaging (IWMPI)*, p. 1, Istanbul, Turkey, 2015.

[30] P. Keselman, E. Y. Yu, X. Y. Zhou et al., "Tracking short-term biodistribution and long-term clearance of SPIO tracers in magnetic particle imaging," *Physics in Medicine and Biology*, vol. 62, no. 9, pp. 3440–3453, 2017.

[31] X. Y. Zhou, K. E. Jeffris, E. Y. Yu et al., "First in vivo magnetic particle imaging of lung perfusion in rats," *Physics in Medicine and Biology*, vol. 62, no. 9, pp. 3510–3522, 2017.

[32] J. Rahmer, A. Antonelli, C. Sfara et al., "Nanoparticle encapsulation in red blood cells enables blood-pool magnetic particle imaging hours after injection," *Physics in Medicine & Biology*, vol. 58, no. 12, pp. 3965–3977, 2013.

[33] B. Zheng, M. P. von See, E. Yu et al., "Quantitative magnetic particle imaging monitors the transplantation, biodistribution, and clearance of stem cells in vivo," *Theranostics*, vol. 6, no. 3, pp. 291–301, 2016.

[34] B. Zheng, T. Vazin, P. W. Goodwill et al., "Magnetic Particle Imaging tracks the long-term fate of *in vivo* neural cell implants with high image contrast," *Scientific Reports*, vol. 5, no. 1, article 14055, 2015.

[35] J. W. Bulte, P. Walczak, M. Janowski et al., "Quantitative "hot spot" imaging of transplanted stem cells using superparamagnetic tracers and magnetic particle imaging (MPI)," *Tomography*, vol. 1, no. 2, pp. 91–97, 2015.

[36] A. Rivera-Rodriguez, L. B. Hoang-Minh, A. Chiu-Lam et al., "Tracking adoptive T cell immunotherapy using magnetic particle imaging," *Nanotheranostics*, vol. 5, no. 4, pp. 431–444, 2021.

[37] A. V. Makela, J. M. Gaudet, M. A. Schott, O. C. Sehl, C. H. Contag, and P. J. Foster, "Magnetic particle imaging of macrophages associated with cancer: filling the voids left by iron-based magnetic resonance imaging," *Molecular Imaging and Biology*, vol. 22, no. 4, pp. 958–968, 2020.

[38] E. Y. Yu, M. Bishop, B. Zheng et al., "Magnetic particle imaging: a novel in vivo imaging platform for cancer detection," *Nano Letters*, vol. 17, no. 3, pp. 1648–1654, 2017.

[39] P. Chandrasekharan, Z. W. Tay, D. Hensley et al., "Using magnetic particle imaging systems to localize and guide magnetic hyperthermia treatment: tracers, hardware, and future medical applications," *Theranostics*, vol. 10, no. 7, pp. 2965–2981, 2020.

[40] Z. W. Tay, S. Savliwala, D. W. Hensley et al., "Superferromagnetic nanoparticles enable order-of-magnitude resolution & sensitivity gain in magnetic particle imaging," *Small Methods*, vol. 5, no. 11, article e2100796, 2021.

[41] M. M. Michenfelder, L. J. Bartlett, D. W. Mahoney, T. J. Herold, and J. C. Hung, "Particle-size and radiochemical purity evaluations of filtered 99mTc-sulfur colloid prepared with different heating times," *Journal of Nuclear Medicine Technology*, vol. 42, no. 4, pp. 283–288, 2014.

[42] K. L. B. Fung, C. Colson, J. Bryan et al., "First superferromagnetic remanence characterization and scan optimization for super-resolution Magnetic Particle Imaging," *Nano Letters*, vol. 23, pp. 1717–1725, 2023.

[43] C. Colson, K. B. Fung, J. Bryan et al., "Evidence that SPIO Chain Formation is Essential for High-Resolution MPI," *bioRxiv*, 2022.

[44] J. Lodhia, G. Mandarano, N. Ferris, P. Eu, and S. Cowell, "Development and use of iron oxide nanoparticles (part 1): synthesis of iron oxide nanoparticles for MRI," *Biomedical Imaging and Intervention Journal*, vol. 6, no. 2, 2010.

[45] K. H. Yeo, I. Rodrigo, R. Kuo, P. Chandrasekharan, B. Fellows, and S. Conolly, "Characterizing the performance of commercial magnetic particles for magnetic particle imaging," *International Journal on Magnetic Particle Imaging*, vol. 8, 2022.

[46] M. Unni, A. M. Uhl, S. Savliwala et al., "Thermal decomposition synthesis of iron oxide nanoparticles with diminished magnetic dead layer by controlled addition of oxygen," *ACS Nano*, vol. 11, no. 2, pp. 2284–2303, 2017.

[47] J. Bryan, B. Fellows, K. B. Fung, P. Chandrasekharan, and S. Conolly, "Optimizing magnetic particle image resolution using superferromagnetic nanoparticles modified through post-synthesis oxidation," *International Journal on Magnetic Particle Imaging*, vol. 8, 2022.

[48] J. P. Bullivant, S. Zhao, B. J. Willenberg, B. Kozissnik, C. D. Batich, and J. Dobson, "Materials characterization of Feraheme/ferumoxytol and preliminary evaluation of its potential for magnetic fluid hyperthermia," *International Journal of Molecular Sciences*, vol. 14, no. 9, pp. 17501–17510, 2013.

[49] P. Reimer and T. Balzer, "Ferucarbotran (Resovist): a new clinically approved RES-specific contrast agent for contrast-enhanced MRI of the liver: properties, clinical development, and applications," *European Radiology*, vol. 13, no. 6, pp. 1266–1276, 2003.

[50] C. E. Mullins, "Magnetic susceptibility of the soil and its significance in soil science – a review," *Journal of Soil Science*, vol. 28, no. 2, pp. 223–246, 1977.

[51] Z. W. Tay, D. W. Hensley, E. C. Vreeland, B. Zheng, and S. M. Conolly, "The relaxation wall: experimental limits to improving MPI spatial resolution by increasing nanoparticle core size," *Biomedical Physics & Engineering Express*, vol. 3, no. 3, article 035003, 2017.

[52] Z. W. Tay, D. Hensley, J. Ma et al., "Pulsed excitation in magnetic particle imaging," *IEEE Transactions on Medical Imaging*, vol. 38, no. 10, pp. 2389–2399, 2019.

[53] Q. Wang, X. Ma, H. Liao et al., "Artificially engineered cubic iron oxide nanoparticle as a high-performance magnetic particle imaging tracer for stem cell tracking," *ACS Nano*, vol. 14, no. 2, pp. 2053–2062, 2020.

[54] S. K. Avugadda, S. Wickramasinghe, D. Niculaes et al., "Uncovering the magnetic particle imaging and magnetic resonance imaging features of iron oxide Nanocube clusters," *Nanomaterials*, vol. 11, no. 1, p. 62, 2021.

[55] H. Daniel, T. Zhi Wei, D. Rohan et al., "Combining magnetic particle imaging and magnetic fluid hyperthermia in a theranostic platform," *Physics in Medicine & Biology*, vol. 62, no. 9, pp. 3483–3500, 2017.

[56] R. Dhavalikar and C. Rinaldi, "Theoretical predictions for spatially-focused heating of magnetic nanoparticles guided by magnetic particle imaging field gradients," *Journal of Magnetism and Magnetic Materials*, vol. 419, pp. 267–273, 2016.

[57] Z. W. Tay, P. Chandrasekharan, A. Chiu-Lam et al., "Magnetic Particle Imaging Guided Heating In Vivo using Gradient Fields For Arbitrary Localization of Magnetic Hyperthermia Therapy," *ACS Nano*, vol. 12, no. 4, pp. 3699–3713, 2018.

[58] A. Antonelli, P. Szwargulski, E.-S. Scarpa et al., "Development of long circulating magnetic particle imaging tracers: use of novel magnetic nanoparticles and entrapment into human erythrocytes," *Nanomedicine*, vol. 15, no. 8, pp. 739–753, 2020.

[59] L. C. Wu, Y. Zhang, G. Steinberg et al., "A review of magnetic particle imaging and perspectives on neuroimaging," *American Journal of Neuroradiology*, vol. 40, no. 2, pp. 206–212, 2019.

[60] K. O. Jung, H. Jo, J. H. Yu, S. S. Gambhir, and G. Pratx, "Development and MPI tracking of novel hypoxia-targeted theranostic exosomes," *Biomaterials*, vol. 177, pp. 139–148, 2018.

[61] M. I. Ramirez, M. G. Amorim, C. Gadelha et al., "Technical challenges of working with extracellular vesicles," *Nanoscale*, vol. 10, no. 3, pp. 881–906, 2018.

[62] B. Gleich, "The Focus Field," in *Principles and Applications of Magnetic Particle Imaging. Aktuelle Forschung Medizintechnik*, B. Gleich, Ed., pp. 45–47, Springer Vieweg, Wiesbaden, 2014.

[63] B. Gleich, "Resolution, sensitivity and speed," in *Principles and Applications of Magnetic Particle Imaging. Aktuelle Forschung Medizintechnik*, B. Gleich, Ed., pp. 49–68, Springer Vieweg, Wiesbaden, 2014.

[64] P. W. Goodwill and S. M. Conolly, *Techniques for Magnetic Particle Imaging*, 2021, U.S. Patent 11,054,392.

[65] P. W. Goodwill, J. J. Konkle, B. Zheng, E. U. Saritas, and S. M. Conolly, "Projection x-space magnetic particle imaging," *IEEE Transactions on Medical Imaging*, vol. 31, no. 5, pp. 1076–1085, 2012.

[66] P. W. Goodwill, E. U. Saritas, L. R. Croft et al., "X-space MPI: magnetic nanoparticles for safe medical imaging," *Advanced Materials*, vol. 24, no. 28, pp. 3870–3877, 2012.

[67] P. W. Goodwill, A. Tamrazian, L. R. Croft et al., "Ferrohydrodynamic relaxometry for magnetic particle imaging," *Applied Physics Letters*, vol. 98, no. 26, article 262502, 2011.

[68] J. Sedlacik, A. Frölich, J. Spallek et al., "Magnetic particle imaging for high temporal resolution assessment of aneurysm hemodynamics," *PLoS One*, vol. 11, no. 8, article e0160097, 2016.

[69] P. Vogel, M. A. Rückert, P. Klauer, W. H. Kullmann, P. M. Jakob, and V. C. Behr, "Traveling wave magnetic particle imaging," *IEEE Transactions on Medical Imaging*, vol. 33, no. 2, pp. 400–407, 2014.

[70] T. Knopp, T. F. Sattel, S. Biederer et al., "Model-based reconstruction for magnetic particle imaging," *IEEE Transactions on Medical Imaging*, vol. 29, no. 1, pp. 12–18, 2010.

[71] T. Knopp and A. Weber, "Recovery of the magnetic particle imaging system matrix using compressed sensing reconstruction," in *2013 International Workshop on Magnetic Particle Imaging (IWMPI)*, p. 1, Berkeley, CA, USA, 2013.

[72] P. W. Goodwill and S. M. Conolly, "Multidimensional x-space magnetic particle imaging," *IEEE Transactions on Medical Imaging*, vol. 30, no. 9, pp. 1581–1590, 2011.

[73] P. W. Goodwill, K. Lu, B. Zheng, and S. M. Conolly, "An x-space magnetic particle imaging scanner," *Review of Scientific Instruments*, vol. 83, no. 3, article 033708, 2012.

[74] K. Murase, R. Song, and S. Hiratsuka, "Magnetic particle imaging of blood coagulation," *Applied Physics Letters*, vol. 104, no. 25, article 252409, 2014.

[75] A. Halkola, J. Rahmer, B. Gleich, J. Borgert, and T. Buzug, "System calibration unit for magnetic particle imaging: System matrix," in *2013 International Workshop on Magnetic Particle Imaging (IWMPI)*, p. 1, Berkeley, CA, USA, 2013.

[76] T. Knopp and T. M. Buzug, *Magnetic Particle Imaging: An Introduction to Imaging Principles and Scanner Instrumentation*, Springer Science & Business Media, 2012.

[77] B. G. Chae, "Neural network image reconstruction for magnetic particle imaging," *ETRI Journal*, vol. 39, no. 6, pp. 841–850, 2017.

[78] S. Dittmer, T. Kluth, M. T. R. Henriksen, and P. Maass, "Deep image prior for 3D magnetic particle imaging: A quantitative comparison of regularization techniques on Open MPI dataset," 2020, https://arxiv.org/abs/2007.01593.

[79] B. Askin, A. Güngör, D. Alptekin Soydan, E. U. Saritas, C. B. Top, and T. Cukur, "PP-MPI: a deep plug-and-play prior for magnetic particle imaging reconstruction," in *Machine Learning for Medical Image Reconstruction. MLMIR 2022*, N. Haq, P. Johnson, A. Maier, C. Qin, T. Würfl, and J. Yoo, Eds., vol. 13587 of Lecture Notes in Computer Science, pp. 105–114, Springer, Cham, 2022.

[80] Y. Shang, J. Liu, L. Zhang et al., "Deep learning for improving the spatial resolution of magnetic particle imaging," *Physics in Medicine & Biology*, vol. 67, no. 12, article 125012, 2022.

[81] T. Knopp, P. Szwargulski, F. Griese, and M. Gräser, "OpenMPIData: an initiative for freely accessible magnetic particle imaging data," *Data in Brief*, vol. 28, article 104971, 2020.

[82] H. Hayat, A. Sun, H. Hayat et al., "Artificial intelligence analysis of magnetic particle imaging for islet transplantation in a mouse model," *Molecular Imaging and Biology.*, vol. 23, no. 1, pp. 18–29, 2021.

[83] D. Hensley, P. Goodwill, L. Croft, and S. Conolly, "Preliminary experimental X-space color MPI," in *2015 5th International Workshop on Magnetic Particle Imaging (IWMPI)*, p. 1, Istanbul, Turkey, 2015.

[84] Z. W. Tay, S. Savliwala, D. Hensley et al., "Superferromagnetic iron oxide: a new paradigm for color multiplex and FRET-like nanoscale 'ruler' for magnetic particle imaging," in *Colloidal Nanoparticles for Biomedical Applications XVII*, pp. 18–23, San Francisco, California, US, 2022.

[85] M. T. Arslan, A. A. Özaslan, S. Kurt, Y. Muslu, and E. U. Saritas, "Rapid TAURUS for relaxation-based color magnetic particle imaging," *IEEE Transactions on Medical Imaging*, vol. 41, no. 12, pp. 3774–3786, 2022.

[86] R. Kuo, C. Saayuja, K. H. Yeo et al., "Brownian superparamagnetic nanoparticles for cell viability assessment in Magnetic Particle Imaging, International Journal on Magnetic

Particle Imaging," in *Proceedings of IWMPI*, Aachen, Germany, 2023.

[87] M. Utkur and E. U. Saritas, "Simultaneous temperature and viscosity estimation capability via magnetic nanoparticle relaxation," *Medical Physics*, vol. 49, no. 4, pp. 2590–2601, 2022.

[88] E. U. Saritas, P. W. Goodwill, G. Z. Zhang, and S. M. Conolly, "Magnetostimulation limits in magnetic particle imaging," *IEEE Transactions on Medical Imaging*, vol. 32, no. 9, pp. 1600–1610, 2013.

[89] R. Weissleder, D. D. Stark, B. L. Engelstad et al., "Superparamagnetic iron oxide: pharmacokinetics and toxicity," *American Journal of Roentgenology*, vol. 152, no. 1, pp. 167–173, 1989.

[90] D. Pouliquen, J. J. Le Jeune, R. Perdrisot, A. Ermias, and P. Jallet, "Iron oxide nanoparticles for use as an MRI contrast agent: pharmacokinetics and metabolism," *Magnetic Resonance Imaging*, vol. 9, no. 3, pp. 275–283, 1991.

[91] M. Lu, M. H. Cohen, D. Rieves, and R. Pazdur, "FDA report: Ferumoxytol for intravenous iron therapy in adult patients with chronic kidney disease," *American Journal of Hematology*, vol. 85, no. 5, pp. 315–319, 2010.

[92] J. Guzy, S. Chakravarty, F. J. Buchanan et al., "Complex relationship between iron oxide nanoparticle degradation and the signal intensity in magnetic particle imaging," *ACS Applied Nano Materials*, vol. 3, no. 5, pp. 3991–3999, 2020.

[93] S. Metzler, D. Stentz, L. Johnson, P. Sankar, and M. Guerraty, "Phantom evaluation of C-SPECT performance for myocardial perfusion imaging," in *2020 IEEE Nuclear Science Symposium and Medical Imaging Conference (NSS/MIC)*, Boston, MA, USA, 2020.

[94] D. J. Brenner and E. J. Hall, "Computed tomography — an increasing source of radiation exposure," *New England Journal of Medicine*, vol. 357, no. 22, pp. 2277–2284, 2007.

[95] H. A. Ziessman, J. P. O'Malley, and J. H. Thrall, "Chapter 7 - hepatobiliary system," in *Nuclear Medicine*, H. A. Ziessman, J. P. O'Malley, and J. H. Thrall, Eds., pp. 159–214, Mosby, Philadelphia, 3rd edition, 2006.

[96] A. P. Khandhar, P. Keselman, S. J. Kemp et al., "Evaluation of PEG-coated iron oxide nanoparticles as blood pool tracers for preclinical magnetic particle imaging," *Nanoscale*, vol. 9, no. 3, pp. 1299–1306, 2017.

[97] A. Antonelli and M. Magnani, "Red Blood Cells Constructs to Prolong the Life Span of Iron-Based Magnetic Resonance Imaging/Magnetic Particle Imaging Contrast Agents In Vivo," in *Clinical Applications of Magnetic Nanoparticles*, pp. 431–450, CRC Press, 2018.

[98] H. L. Liu, Y. Pu, L. D. Nickerson, Y. Liu, P. T. Fox, and J. H. Gao, "Comparison of the temporal response in perfusion and BOLD-based event-related functional MRI," *Magnetic Resonance in Medicine*, vol. 43, no. 5, pp. 768–772, 2000.

[99] K. L. Leenders, D. Perani, A. A. Lammertsma et al., "Cerebral blood flow, blood volume and oxygen utilization. Normal values and effect of age," *Brain*, vol. 113, pp. 27–47, 1990.

[100] O. B. Paulson, S. G. Hasselbalch, E. Rostrup, G. M. Knudsen, and D. Pelligrino, "Cerebral blood flow response to functional activation," *Journal of Cerebral Blood Flow and Metabolism*, vol. 30, no. 1, pp. 2–14, 2010.

[101] S. T. Francis, J. A. Pears, S. Butterworth, R. W. Bowtell, and P. A. Gowland, "Measuring the change in CBV upon cortical activation with high temporal resolution using look-locker EPI and Gd-DTPA," *Magnetic Resonance in Medicine*, vol. 50, no. 3, pp. 483–492, 2003.

[102] T. Kim, K. S. Hendrich, K. Masamoto, and S. G. Kim, "Arterial versus total blood volume changes during neural activity-induced cerebral blood flow change: implication for BOLD fMRI," *Journal of Cerebral Blood Flow and Metabolism*, vol. 27, no. 6, pp. 1235–1247, 2007.

[103] J. B. Mandeville, B. G. Jenkins, B. E. Kosofsky, M. A. Moskowitz, B. R. Rosen, and J. J. Marota, "Regional sensitivity and coupling of BOLD and CBV changes during stimulation of rat brain," *Magnetic Resonance in Medicine*, vol. 45, no. 3, pp. 443–447, 2001.

[104] S. N. Krieger, M. N. Streicher, R. Trampel, and R. Turner, "Cerebral blood volume changes during brain activation," *Journal of Cerebral Blood Flow & Metabolism*, vol. 32, no. 8, pp. 1618–1631, 2012.

[105] S. D. Keilholz, A. C. Silva, M. Raman, H. Merkle, and A. P. Koretsky, "BOLD and CBV-weighted functional magnetic resonance imaging of the rat somatosensory system," *Magnetic Resonance in Medicine*, vol. 55, no. 2, pp. 316–324, 2006.

[106] H. Lu, X. Golay, J. J. Pekar, and P. C. Van Zijl, "Functional magnetic resonance imaging based on changes in vascular space occupancy," *Magnetic Resonance in Medicine*, vol. 50, no. 2, pp. 263–274, 2003.

[107] R. Orendorff, M. Wendland, E. Yu, B. Zheng, P. Goodwill, and S. Conolly, "First in vivo brain perfusion imaging using magnetic particle imaging," in *2016 World Molecular Imaging Congress (WMIC 2016): Imaging Biology Improving Therapy*, New York, USA, 2016.

[108] C. Z. Cooley, J. B. Mandeville, E. E. Mason, E. T. Mandeville, and L. L. Wald, "Rodent cerebral blood volume (CBV) changes during hypercapnia observed using magnetic particle imaging (MPI) detection," *NeuroImage*, vol. 178, pp. 713–720, 2018.

[109] P. Ludewig, N. Gdaniec, J. Sedlacik et al., "Magnetic particle imaging for real-time perfusion imaging in acute stroke," *ACS Nano*, vol. 11, no. 10, pp. 10480–10488, 2017.

[110] P. Szwargulski, M. Wilmes, E. Javidi et al., "Monitoring intracranial cerebral hemorrhage using multicontrast real-time magnetic particle imaging," *ACS Nano*, vol. 14, no. 10, pp. 13913–13923, 2020.

[111] B. W. Carney, G. Khatri, and A. S. Shenoy-Bhangle, "The role of imaging in gastrointestinal bleed," *Cardiovascular Diagnosis and Therapy*, vol. 9, no. S1, pp. S88–s96, 2019.

[112] Y. Mariam, C. Prashant, and C. Steven, "Magnetic Particle Imaging for the Evaluation of Gastrointestinal Health by Measuring Gastrointestinal Permeability, International Journal on Magnetic Particle Imaging," in *Proceedings of IWMPI*, Aachen, Germany, 2023.

[113] H. Wei, J. Shang, C. Keohane et al., "A novel approach to assess the spontaneous gastrointestinal bleeding risk of antithrombotic agents using Apc(min/+) mice," *Thrombosis and Haemostasis*, vol. 111, no. 6, pp. 1121–1132, 2014.

[114] L. Wang and Q. Zhang, "Application of the $Apc^{Min/+}$ mouse model for studying inflammation-associated intestinal tumor," *Biomedicine & Pharmacotherapy*, vol. 71, pp. 216–221, 2015.

[115] A. T. Cohen, G. Agnelli, F. A. Anderson et al., "Venous thromboembolism (VTE) in Europe. The number of VTE events and associated morbidity and mortality," *Thrombosis and Haemostasis*, vol. 98, no. 4, pp. 756–764, 2007.

[116] C. Kearon, "Diagnosis of pulmonary embolism," *CMAJ*, vol. 168, no. 2, pp. 183–194, 2003.

[117] P. F. Fedullo and V. F. Tapson, "The evaluation of suspected pulmonary embolism," *The New England Journal of Medicine*, vol. 349, no. 13, pp. 1247–1256, 2003.

[118] G. P. Schembri, A. E. Miller, and R. Smart, "Radiation dosimetry and safety issues in the investigation of pulmonary embolism," *Seminars in Nuclear Medicine*, vol. 40, no. 6, pp. 442–454, 2010.

[119] B. Ghaye, A. Ghuysen, P. J. Bruyere, V. D'Orio, and R. F. Dondelinger, "Can CT pulmonary angiography allow assessment of severity and prognosis in patients presenting with pulmonary embolism? What the radiologist needs to know," *Radiographics*, vol. 26, no. 1, pp. 23–39, 2006.

[120] J. Bělohlávek, V. Dytrych, and A. Linhart, "Pulmonary embolism, part I: epidemiology, risk factors and risk stratification, pathophysiology, clinical presentation, diagnosis and nonthrombotic pulmonary embolism," *Experimental and Clinical Cardiology*, vol. 18, no. 2, pp. 129–138, 2013.

[121] D. Pantke, F. Mueller, S. Reinartz, F. Kiessling, and V. Schulz, "Flow velocity quantification by exploiting the principles of the Doppler effect and magnetic particle imaging," *Scientific Reports*, vol. 11, no. 1, article 4529, 2021.

[122] P. M. Chisholm, H. J. Danpure, G. Healey, and S. Osman, "Cell damage resulting from the labeling of rat lymphocytes and HeLa S3 cells with in-111 oxine," *Journal of Nuclear Medicine*, vol. 20, no. 12, pp. 1308–1311, 1979.

[123] National Library of Medicine (US), "National Center for Biotechnology Information. Indium In 111 oxyquinoline," PubChem Compound Summary for CID 119117, Bethesda (MD), 2004, https://pubchem.ncbi.nlm.nih.gov/compound/Indium-In-111-oxyquinoline.

[124] D. A. Goodwin, "Cell labeling with oxine chelates of radioactive metal ions: techniques and clinical implications," *Journal of Nuclear Medicine*, vol. 19, pp. 557–559, 1978.

[125] N. C. Manley and G. K. Steinberg, "Tracking stem cells for cellular therapy in stroke," *Current Pharmaceutical Design*, vol. 18, no. 25, pp. 3685–3693, 2012.

[126] J. W. M. Bulte and H. E. Daldrup-Link, "Clinical tracking of cell transfer and cell transplantation: trials and tribulations," *Radiology*, vol. 289, no. 3, pp. 604–615, 2018.

[127] P. Wang, P. W. Goodwill, P. Pandit et al., "Magnetic particle imaging of islet transplantation in the liver and under the kidney capsule in mouse models," *Quantitative Imaging in Medicine and Surgery*, vol. 8, no. 2, pp. 114–122, 2018.

[128] O. C. Sehl, A. V. Makela, A. M. Hamilton, and P. J. Foster, "Trimodal cell tracking in vivo: combining iron- and fluorine-based magnetic resonance imaging with magnetic particle imaging to monitor the delivery of mesenchymal stem cells and the ensuing inflammation," *Tomography*, vol. 5, no. 4, pp. 367–376, 2019.

[129] H. Nejadnik, P. Pandit, O. Lenkov, A. P. Lahiji, K. Yerneni, and H. E. Daldrup-Link, "Ferumoxytol can be used for quantitative magnetic particle imaging of transplanted stem cells," *Molecular Imaging and Biology*, vol. 21, no. 3, pp. 465–472, 2019.

[130] N. Pandit-Taskar, M. A. Postow, M. D. Hellmann et al., "First-in-humans imaging with (89)Zr-Df-IAB22M2C anti-CD8 Minibody in patients with solid malignancies: preliminary pharmacokinetics, biodistribution, and lesion targeting," *Journal of Nuclear Medicine*, vol. 61, no. 4, pp. 512–519, 2020.

[131] F. Petitprez, M. Meylan, A. de Reyniès, C. Sautès-Fridman, and W. H. Fridman, "The tumor microenvironment in the response to immune checkpoint blockade therapies," *Frontiers in Immunology*, vol. 11, p. 784, 2020.

[132] D. Borsetto, M. Tomasoni, K. Payne et al., "Prognostic significance of CD4+ and CD8+ tumor-infiltrating lymphocytes in head and neck squamous cell carcinoma: a meta-analysis," *Cancers*, vol. 13, no. 4, p. 781, 2021.

[133] S. B. Coffelt, M. D. Wellenstein, and K. E. de Visser, "Neutrophils in cancer: neutral no more," *Nature Reviews Cancer*, vol. 16, no. 7, pp. 431–446, 2016.

[134] L. Wu and X. H. Zhang, "Tumor-associated neutrophils and macrophages-heterogenous but not chaotic," *Frontiers in Immunology*, vol. 11, article 553967, 2020.

[135] E. Obeid, R. Nanda, Y.-X. Fu, and O. I. Olopade, "The role of tumor-associated macrophages in breast cancer progression," *International Journal of Oncology*, vol. 43, no. 1, pp. 5–12, 2013.

[136] M. A. Miller, S. Arlauckas, and R. Weissleder, "Prediction of anti-cancer Nanotherapy efficacy by imaging," *Nanotheranostics*, vol. 1, no. 3, pp. 296–312, 2017.

[137] R. Kuo, P. Chandrasekharan, B. Fung, and S. Conolly, "In vivo therapeutic cell tracking using magnetic particle imaging," *International Journal on Magnetic Particle Imaging*, vol. 8, 2022.

[138] K. B. Fung, P. Chandrasekharan, X. Y. Zhou, W. Cui, L. Fong, and S. Conolly, "Rapid in situ labelling and tracking of neutrophils and macrophages to inflammation using antibody-functionalized MPI tracers," *International Journal on Magnetic Particle Imaging*, vol. 8, 2022.

[139] L. T. Baxter, H. Zhu, D. G. Mackensen, W. F. Butler, and R. K. Jain, "Biodistribution of monoclonal antibodies: scale-up from mouse to human using a physiologically based pharmacokinetic model," *Cancer Research*, vol. 55, no. 20, pp. 4611–4622, 1995.

[140] N. Baririan, "Monoclonal antibodies: clinical pharmacology keys," *Applied Clinical Trials*, vol. 27, 2018.

[141] K. Nakamura and A. Kubo, "Biodistribution of iodine-125 labeled monoclonal antibody/Interleukin-2 immunoconjugate in athymic mice bearing human tumor xenografts," *Cancer*, vol. 80, no. S12, pp. 2650–2655, 1997.

[142] M. L. Thakur and J. D. DeFulvio, "Technetium-99m-labeled monoclonal antibodies for immunoscintigraphy: simplified preparation and evaluation," *Journal of Immunological Methods*, vol. 137, no. 2, pp. 217–224, 1991.

[143] E. Vegt, M. de Jong, J. F. Wetzels et al., "Renal toxicity of radiolabeled peptides and antibody fragments: mechanisms, impact on radionuclide therapy, and strategies for prevention," *Journal of Nuclear Medicine*, vol. 51, no. 7, pp. 1049–1058, 2010.

[144] J. Zhong, C. Zheng, H. Gao, W. Tong, H. Hui, and J. Tian, "Noninvasive imaging of the lung NETosis by anti-Ly6G iron oxide nanoparticles," *Heliyon*, vol. 8, no. 8, article e10043, 2022.

[145] G. Ren, J. M. Gaudet, M. Gerosa et al., "Abstract 2770: imaging cancer immunology: monitoring CD47 mAb treatment in vivo by magnetic particle imaging," *Cancer Research*, vol. 80, Supplement 16, p. 2770, 2020.

[146] B. Fisher, B. S. Packard, E. J. Read et al., "Tumor localization of adoptively transferred indium-111 labeled tumor infiltrating lymphocytes in patients with metastatic melanoma," *Journal of Clinical Oncology*, vol. 7, no. 2, pp. 250–261, 1989.

[147] K. D. Griffith, E. J. Read, J. A. Carrasquillo et al., "In vivo distribution of adoptively transferred indium-111-labeled tumor infiltrating lymphocytes and peripheral blood lymphocytes in patients with metastatic melanoma," *Journal of the National Cancer Institute*, vol. 81, no. 22, pp. 1709–1717, 1989.

[148] R. Kuo, B. Fung, P. Chandrasekharan et al., "Non-radioactive imaging of bone marrow using antibody-conjugated nanoparticles in magnetic particle imaging," *International Journal on Magnetic Particle Imaging*, vol. 8, 2022.

[149] E. A. Olsen, S. Whittaker, Y. H. Kim et al., "Clinical end points and response criteria in mycosis fungoides and Sézary syndrome: a consensus statement of the International Society for Cutaneous Lymphomas, the United States cutaneous lymphoma consortium, and the cutaneous lymphoma task force of the European Organisation for Research and Treatment of Cancer," *Journal of Clinical Oncology*, vol. 29, no. 18, pp. 2598–2607, 2011.

[150] B. D. Cheson, R. I. Fisher, S. F. Barrington et al., "Recommendations for initial evaluation, staging, and response assessment of Hodgkin and non-Hodgkin lymphoma: The Lugano classification," *Journal of Clinical Oncology*, vol. 32, no. 27, pp. 3059–3067, 2014.

[151] L. Kiru, A. Zlitni, A. M. Tousley et al., "In vivo imaging of nanoparticle-labeled CAR T cells," *Proceedings of the National Academy of Sciences.*, vol. 119, no. 6, article e2102363119, 2022.

[152] J. H. Choe, P. B. Watchmaker, M. S. Simic et al., "SynNotch-CAR T cells overcome challenges of specificity, heterogeneity, and persistence in treating glioblastoma," *Science Translational Medicine*, vol. 13, no. 591, p. 13, 2021.

[153] Z. W. Tay, P. Chandrasekharan, B. D. Fellows et al., "Magnetic particle imaging: an emerging modality with prospects in Diagnosis, Targeting and Therapy of Cancer," *Cancers*, vol. 13, no. 21, p. 5285, 2021.

[154] W. Tong, H. Hui, W. Shang et al., "Highly sensitive magnetic particle imaging of vulnerable atherosclerotic plaque with active myeloperoxidase-targeted nanoparticles," *Theranostics*, vol. 11, no. 2, pp. 506–521, 2021.

[155] X. Zhu, J. Li, P. Peng, N. Hosseini Nassab, and B. R. Smith, "Quantitative drug release monitoring in tumors of living subjects by magnetic particle imaging nanocomposite," *Nano Letters*, vol. 19, no. 10, pp. 6725–6733, 2019.

[156] M. Ju, M. Navarreto-Lugo, S. Wickramasinghe, N. B. Milbrandt, A. McWhorter, and A. C. S. Samia, "Exploring the chelation-based plant strategy for iron oxide nanoparticle uptake in garden cress (Lepidium sativum) using magnetic particle spectrometry," *Nanoscale*, vol. 11, no. 40, pp. 18582–18594, 2019.

[157] A. Neumann, K. Gräfe, A. von Gladiss et al., "Recent developments in magnetic particle imaging," *Journal of Magnetism and Magnetic Materials*, vol. 550, article 169037, 2022.

[158] J. Pagan, C. McDonough, T. Vo, and A. Tonyushkin, "Single-sided magnetic particle imaging device with Field-free-line geometry for in-vivo imaging applications," *IEEE Transactions on Magnetics*, vol. 57, no. 2, pp. 1–5, 2021.